Elektronica en Telecommunicatie 7

Gemeenschappelijke publikatie van de Sectie voor Telecommunicatietechniek van het KIvI en het Nederlands Elektronica- en Radiogenootschap.

Redactie-adres: Prinsessegracht 23, Den Haag.

Symposium Antennas

621.396.67

IV. Absorption and Scattering Properties of Antennas in Relation to the Application of the Van Atta Principle

by ir. E. P. W. Attema, Microwave Laboratory, Department of Electrical Engineering, Delft University of Technology



Synopsis: The physical mechanism of absorption and scattering by antennas is treated in terms of a scattering matrix representation of the antenna. Conditions will be given for which perfect absorption without scattering is obtained. The consequences of satisfying these conditions are studied with respect to the application of the Van Atta principle, for which the scattering properties of antennas are of major interest.

1. Introduction

It is well known that in general a receiving antenna does not only absorb power from an incident electromagnetic wave but scatters in several directions as well. The problem of absorption and scattering by antennas can be formulated in two different ways. One can derive power relations from the relevant electromagnetic field quantities or alternatively from matrix quantities using a network representation of the antenna. In the latter case it is convenient to represent the antenna by a scattering matrix S, the elements of which are the coefficients of an expansion of the electromagnetic fields into complete sets of orthogonal modes in the medium surrounding the antenna as well as on well defined cross-sections of the feeders connected to the antenna.

The physical mechanism of power absorption by a receiving antenna as it depends on the antenna configuration and the incident fieldpattern, will be discussed in this paper in terms of the matrix representation, and conditions will be given under which perfect absorption without scattering occurs. Some authors have arrived at the conclusion that there will always be at least as much power scattering as there is power absorption, while others assert this is not true. In section 3 of this paper arguments are developed in support of the latter point of view [1, 2, 3].

In practice, absorption and scattering properties of antennas are important not only for applications where optimum antenna performance is required, but especially for those applications where scattering causes unwanted disturbances as is, for instance, the case with the so-called Van Atta reflector discussed in the last section.

2. The scattering matrix

The properties of antennas are considered based on a scattering matrix representation of the antenna; the fields around the antenna being specified as a superposition of spherical modes. Since this representation is somewhat unconventional and may be unfamiliar at least to some readers, it may be useful to begin by examining certain underlying principles.

The total electromagnetic field in a vacuum can be expanded into a complete set of orthogonal spherical modes [1] which are solutions of the vector wave equation.

$$\nabla^2 \underline{E} - c^2 \frac{\delta^2 \underline{E}}{\delta t^2} = 0$$

Lectures delivered at the symposium on antennas, organized by the NERG on 18 May 1971 at Delft University of Technology, Department of Electrical Engineering. Former lectures are published in 'De Ingenieur', 1972, no. 20 and no. 24. For the announcement see 'De Ingenieur' 1971, no. 19, p. A 336.

Assuming single-frequency operation, the solutions can be generated by means of the solutions of the scalar wave equation in spherical co-ordinates (Fig. 1).

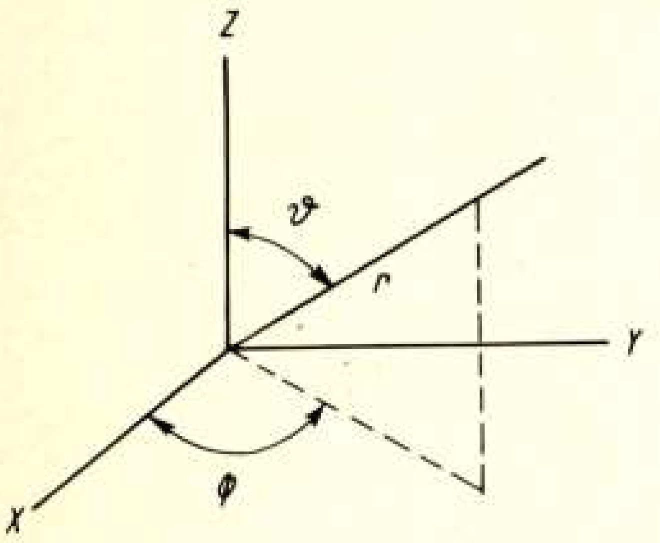


Fig. 1. Spherical co-ordinates.

$x = r \sin \vartheta \cos\varphi$	$0 \leqslant \varphi \leqslant 2\pi$
$y = r \sin \vartheta \sin\varphi$	$0 \leqslant \vartheta \leqslant \pi$
$z = r \cos \vartheta$	$0 \leqslant r < \infty$

$$\frac{1}{r^2}\frac{\delta}{\delta r}\left(r^2\frac{\delta u}{\delta r}\right)+\frac{1}{r^2 \sin\theta}\frac{\delta}{\delta\theta}\left(\sin\theta\frac{\delta u}{\delta\theta}\right)+\frac{1}{r^2\sin^2\theta}\frac{\delta^2 u}{\delta\phi^2}+k^2u=0.$$

The solutions are:

$$u_{m,n}=P_n^{|m|}(\cos\theta)\,e^{jm\varphi}\frac{1}{\sqrt{kr}}Z_{n+\frac{1}{2}}(kr),$$

where:

n, m	=	integers such that $n \geqq 0$, $\lvert m\rvert \leqq n$
P_n^m	=	Legendre polynomials
k	=	wave number
$Z_{n+\frac{1}{2}}$	=	unspecified cylindrical function.

For the vector wave equation two sets of solutions can be constructed:

$$\left.\begin{aligned}\underline{E}(\underline{r},t)&=\sum_{n,m}\mathrm{Re}\,[\underline{r}\times\nabla u_{m,n}\exp(j\omega t)]\\ \underline{H}(\underline{r},t)&=\sum_{n,m}\mathrm{Re}\,[\nabla\times\{\underline{r}\times\nabla u_{m,n}\exp(j\omega t)\}]\end{aligned}\right\}\quad(1)$$

Because $\underline{r}\times\nabla u_{mn}$ is normal to $\underline{r}$ these solutions are called *transverse electric*, whereas

$$\left.\begin{aligned}\underline{H}(\underline{r},t)&=\sum_{n,m}\mathrm{Re}\,[\underline{r}\times\nabla u_{m,n}\exp(j\omega t)]\\ \underline{E}(\underline{r},t)&=\sum_{n,m}\mathrm{Re}\,[\nabla\times\{\underline{r}\times\nabla u_{m,n}\exp(j\omega t)\}]\end{aligned}\right\}\quad(2)$$

for the same reason are called *transverse magnetic*.

It can be proved that (1) and (2) represent a complete set of orthogonal solutions of Maxwell's equations where $Z_{n+\frac{1}{2}}$ is a linear combination of two Hankel functions:

$$Z_{n+\frac{1}{2}}(kr)=a\,H^{(1)}_{n+\frac{1}{2}}(kr)+b\,H^{(2)}_{n+\frac{1}{2}}(kr)$$

The total solution may be expressed as follows:

$$\underline{E}(\underline{r},t)=\sum_{n,m}\mathrm{Re}[\underline{r}\times\nabla\{P_n^{|m|}(\cos\theta)\,e^{jm\varphi}\frac{1}{\sqrt{kr}}a^{TE}_{n,m}H^{(1)}_{n+\frac{1}{2}}(kr)\}]+$$

$$+\sum_{n,m}\left[\nabla\times[\underline{r}\times\{P_n^{|m|}(\cos\theta)\,e^{jm\varphi}\frac{1}{\sqrt{kr}}a^{TM}_{n,m}H^{(1)}_{n+\frac{1}{2}}(kr)\}]\right]+$$

$$+\sum_{n,m}\mathrm{Re}\,[\underline{r}\times\nabla\{P_n^{|m|}(\cos\theta)\,e^{jm\varphi}\frac{1}{\sqrt{kr}}b^{TE}_{n,m}H^{(2)}_{n+\frac{1}{2}}(kr)\}]+$$

$$+\sum_{n,m}\mathrm{Re}\left[\nabla\times[\underline{r}\times\{P_n^{|m|}(\cos\theta)\,e^{jm\varphi}\frac{1}{\sqrt{kr}}b^{TM}_{n,m}H^{(2)}_{n+\frac{1}{2}}(kr)\}]\right].$$

It is important to understand the physical meaning of this solution. It may be seen that, with respect to the θ and φ dependence, the total electromagnetic field has been expanded in orthogonal modes. This means that the power entering or leaving a spherical surface around the origin is equal to the sum of the powers computed for each mode separately. Each mode consists of a pair of terms representing travelling waves that either converge upon the origin or diverge from it. This conclusion is reached on the basis of the explicit asymptotic expressions of $H^{(1)}$ and $H^{(2)}$ for large values of the argument [4]. The relative strengths of these waves are determined by the coefficients a and b. Consequently $\underline{E}(\underline{r},t)$ may be specified as follows: by a converging and a diverging component

$$\underline{E}(\underline{r},t)=\underline{E}^c(\underline{r},t)+\underline{E}^d(\underline{r},t).$$

It is convenient to introduce the following abbreviations:

$$\underline{M}^{TE}_{n,m}=\underline{r}\times\nabla\left\{P_n^{(m)}(\cos\theta)\,e^{jm\varphi}\frac{1}{\sqrt{kr}}H^{(1)}_{n+\frac{1}{2}}(kr)\right\}$$

$$\underline{M}^{TM}_{n,m}=\nabla\times\underline{M}^{TE}_{n,m}$$

$$\underline{N}^{TE}_{n,m}=\underline{r}\times\nabla\left\{P_n^{(m)}(\cos\theta)\,e^{jm\varphi}\frac{1}{\sqrt{kr}}H^{(2)}_{n+\frac{1}{2}}(kr)\right\}$$

$$\underline{N}^{TM}_{n,m}=\nabla\times\underline{N}^{TE}_{n,m}$$

Instead of the double index n,m a single index s can be used, providing that every value of s corresponds to a specific combination $(n,m)^{TE}$ or $(n,m)^{TM}$ such that

$$\underline{E}^c(\underline{r},t)=\Sigma_s\,\mathrm{Re}[a_s\underline{M}_s\exp(j\omega t)]$$

$$\underline{E}^d(\underline{r},t)=\Sigma_s\,\mathrm{Re}[b_s\underline{N}_s\exp(j\omega t)]$$

If the region of interest includes the origin, the field at the origin must be finite, $Z_{n+\frac{1}{2}}$ must be a Bessel function for which $a_s=b_s$. In that case it can be derived from the above expressions, using unit vector notation, that if

$$\underline{E}^d=E_\vartheta\underline{i}_\vartheta+E_\varphi\underline{i}_\varphi+E_r\underline{i}_r$$

then

$$\underline{E}^c=E_\vartheta\underline{i}_\vartheta+E_\varphi\underline{i}_\varphi-E_r\underline{i}_r.$$

This means, as was expected, that a wave approaching the origin from direction $[\vartheta,\varphi]$ is leaving in the direction $[\vartheta,\varphi+\pi]$.

If there is an antenna at the center of the region, the origin must be excluded; in this case no simple relation exists between a_s

and b_s. The various coefficients a_s and b_s however are linearly related to each other, and it is therefore possible to define a scattering matrix that relates the converging waves to the diverging ones.

In the following discussion we will confine ourselves to an antenna connected to a single mode feeder. We may then introduce the column vectors $\underline{a}$ and $\underline{b}$ to represent the converging and the diverging waves.

$$\underline{a} = \begin{bmatrix} a_1 \\ a_2 \\ a_3 \\ \cdot \\ \cdot \\ \cdot \end{bmatrix} \text{ and } \underline{b} = \begin{bmatrix} b_1 \\ b_2 \\ b_3 \\ \cdot \\ \cdot \\ \cdot \end{bmatrix}$$

where a_1 and b_1 are related to the travelling waves along the feederline entering or leaving the antenna respectively.

The scattering matrix S may be defined such that $\underline{b} = S\underline{a}$. The general properties and conventions related to S are described in the literature [5]. Here it is important to recall that S is reciprocal and that S is unitary for a lossless antenna structure.

The receiving mechanism of an antenna may now be visualized in the following way. Assume an incident electromagnetic field consisting of converging and diverging waves of equal strength. An antenna placed at the origin will change the incident field in several respects. Some modes may remain unmodified in the presence of the antenna, and $a_s = b_s$ for the corresponding values of s. Other modes may be disturbed in such a way that the converging part will be converted partly to diverging waves of other modes, partly to waves travelling to the antenna load along the feeder connected to the antenna.

On the other hand the transmitting mechanism can be looked upon as a transformation of modes on well defined cross-sections of the feeder to diverging field modes in the medium surrounding the antenna.

It should be emphasized that the field expansion used in this section departs basically from other divisions of the field around a receiving aerial more common in the antenna literature [3]. Normally a reradiated $(\underline{E}_r, \underline{H}_r)$ is defined which combines with the incident $(\underline{E}_o, \underline{H}_o)$ to form the resultant $(\underline{E}, \underline{H})$:

$$\underline{E} = \underline{E}_o + \underline{E}_r$$

$$\underline{H} = \underline{H}_o + \underline{H}_r$$

where $(\underline{E}_o \underline{H}_o)$ is the undisturbed field that would be present in the absence of the receiving antenna. This universally accepted definition of the reradiated field entails the paradoxial consequence that a perfect absorber appears to reradiate, the reradiated power being at least equal to the absorbed power [1, 2]. It must be kept in mind however that one cannot assign any physical meaning to the field $(\underline{E}_r, \underline{H}_r)$. Consequently the reradiated power cannot be determined from $(\underline{E}_r, \underline{H}_r)$, as has been pointed out by Midgley [3].

In the next section it will be shown that the expansion in orthogonal modes allows for a relatively simple derivation of the relevant power relations.

3. Power relations

In this section we derive general expressions determining the power incident on a receiving antenna and the amounts of power absorbed and scattered by it. Assume a lossless antenna placed at the origin and connected to a single-mode feeder. The antenna is represented by a scattering matrix S. The situation is schematically indicated in Fig. 2.

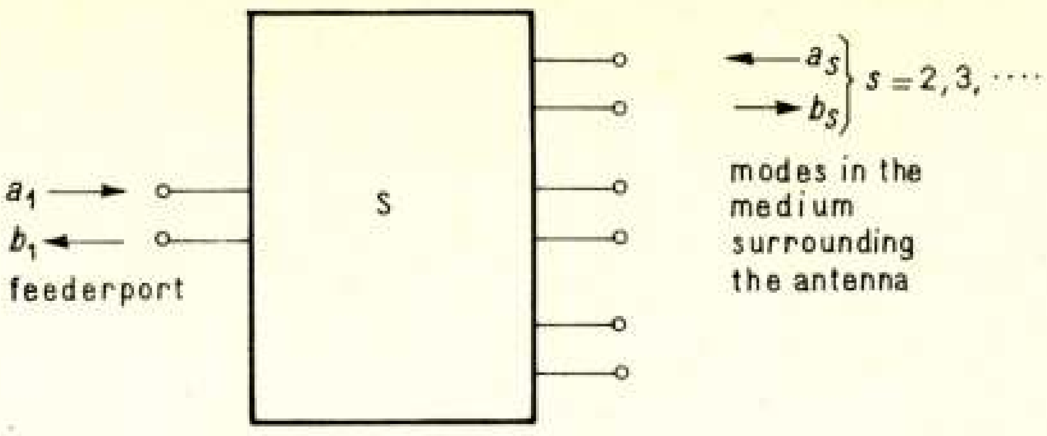


Fig. 2. Scattering matrix representation of an antenna.

$S_{11} = 0$, if the antenna is matched to the feederline.

$$\text{A unit incident wave, } \underline{a} = \begin{bmatrix} 1 \\ 0 \\ 0 \\ \cdot \\ \cdot \\ \cdot \end{bmatrix} \text{ in the feeder port will}$$

$$\text{cause a radiated wave } \underline{b} = \begin{bmatrix} 0 \\ S_{21} \\ S_{31} \\ \cdot \\ \cdot \\ \cdot \end{bmatrix}$$

Apparently the incident power is converted to field modes according to the first row of S, which specifies the radiation pattern of the antenna.

If the antenna is only receiving, $a_1 = 0$ and the incident power is given by:

$$P_i = \frac{1}{2} \sum_{s=2}^{\infty} \left| a_s \right|^2$$

In general this power is transferred partly to the feeder port and partly to other ports. The absorbed power P_A is equal to:

$$\frac{1}{2} \left| b_1 \right|^2 = \frac{1}{2} \sum_{s=3}^{\infty} \left| S_{1s} a_s \right|^2$$

This quantity is determined by the incident wave $\underline{a}$ and the first row of S.

The antenna radiation pattern completely determines the power received from a given incident wave. The remainder of the incident power $P_i - P_A$ is lost. Because of the unitary property of S, a wave incident on an antenna such that $a_s = S_{s1}^*$ ($s = 2, 3, \ldots$) will be completely absorbed without causing a scattering of power since $P_A = P_i$. In this case the incident wave is identical with the wave that the antenna normally radiates except for a time reversal. In practice the possibility of satisfying this condition will be very limited since antenna structures of infinite size might be required.

As an illustration of the above given relations we consider the case of a receiving Hertzian dipole interacting with an incident plane wave. Assume an incident plane wave travelling in the positive Y-direction determined by $\underline{a}$, an infinite-dimensional vector.

$P_i = \frac{1}{2} \sum_{s=2}^{\infty} \left| a_s \right|^2$ is infinite, as it should be for a plane wave

The scattering matrix of a lossless Hertzian dipole, only radiating the first TM-spherical wave and attached to a matched single-mode feeder is

$$S = \begin{bmatrix} 0 & 1 & 0 & - & - & - \\ 1 & 0 & - & - & - & - \\ 0 & - & 1 & & & \\ - & - & & 1 & & \\ - & - & & & 1 & \\ - & - & & & & 1 \end{bmatrix}$$

if the reference plane on the cross-section of the feeder is properly chosen [1]. If the dipole is placed at the origin then $\underline{b} = \mathrm{S}\underline{a}$. The absorbed power P_A is equal to $\frac{1}{2}|b_1|^2 = \frac{1}{2}|a_2|^2$

The power-loss $P_i - P_A$ is equal to $\frac{1}{2} \sum_{s=2}^{\infty} \left| b_s \right|^2 = \frac{1}{2} \sum_{s=3}^{\infty} \left| a_s \right|^2$.

It is important to note here that apparently only the unaffected higher modes of the incident wave contribute to the power-loss.

It is very instructive to consider the resultant field configuration in the present case in more detail.

The incident wave may be divided into a converging and a diverging part $\underline{E} = \underline{E}^c + \underline{E}^d$.
$\underline{E}^c$ is nonzero in the halfspace $0 < \varphi < \pi$ and zero in the halfspace $\pi < \varphi < 2\pi$, whereas $\underline{E}^d(\varphi) = \underline{E}^c(\varphi + \pi)$. This is symbolically indicated in Fig. 3.

The first spherical TM mode absorbed by the dipole is symmetrical about the origin. This means that the resultant field is composed of the undisturbed incident wave from which a symmetrical part is subtracted. From Fig. 3 it may be seen that this results in destructive interference in the halfspace $\pi < \varphi < 2\pi$ and in backscattering in the halfspace $0 < \varphi < \pi$. This conclusion can be proved in general although Fig. 3 is only a simplified symbolic representation of the receiving process.

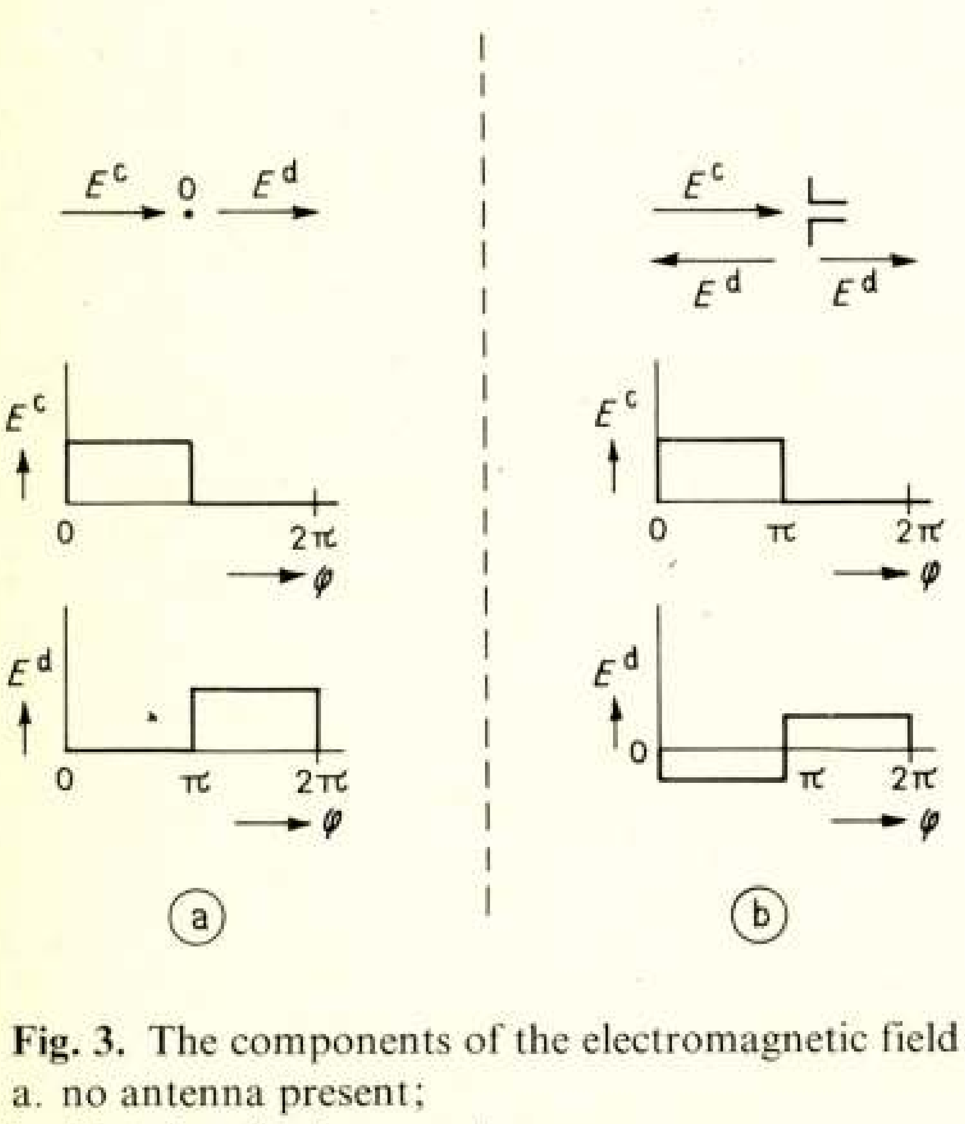


Fig. 3. The components of the electromagnetic field:
a. no antenna present;
b. Hertzian dipole present.

It is clear that for a plane incident wave the Hertzian dipole is far from being the ideal receiving system providing complete absorption without scattering. An incident field configuration consisting of two plane waves of equal strength travelling in opposite directions seems to be more suited for a receiving antenna with symmetrical radiation pattern like the Hertzian dipole, and indeed the Hertzian dipole is able to absorb from such a field four times the power absorbed from a single plane wave of equal strength.

The power lost from a receiving system can be subdivided into backscattering and spill-over loss, depending on the detailed structure of $\underline{E}^d$ compared to the incident wave. In the example above backscattering occurs in the halfspace $0 < \varphi < \pi$ and spill-over loss in the halfspace $\pi < \varphi < 2\pi$. Although it does not affect the power transfer from the incident wave to the antenna load, for special applications it is desirable to minimize the backscattering at the expense of increased spill-over.

4. The Van Atta principle

This section is devoted to the Van Atta reflector as an example of an application where the scattering properties of antennas have special relevance.

In 1959 L. C. van Atta proposed an electromagnetic reflector consisting of an array of antenna elements arranged and interconnected to form a retrodirective reflector [6]. A reflector is called *retrodirective* if it reradiates an incident wave mainly in the direction of its arrival independently of the orientation of the reflector in respect to the propagation vector of the incident wave. The reflector proposed by Van Atta is an array consisting of pairs of antenna elements. These pairs are arranged symmetrically about the array center and the two elements of each pair are interconnected by a matched transmission line. The

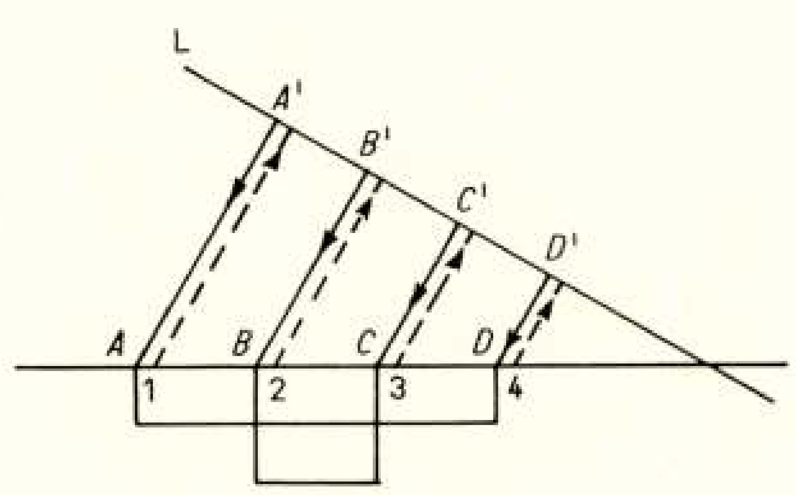


Fig. 4. The Van Atta principle.

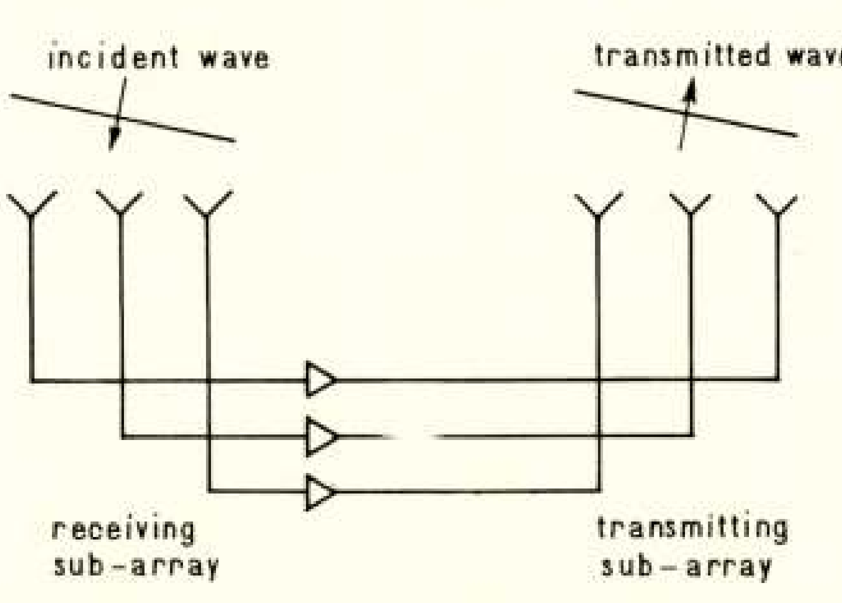


Fig. 5. A variant of the Van Atta reflector.

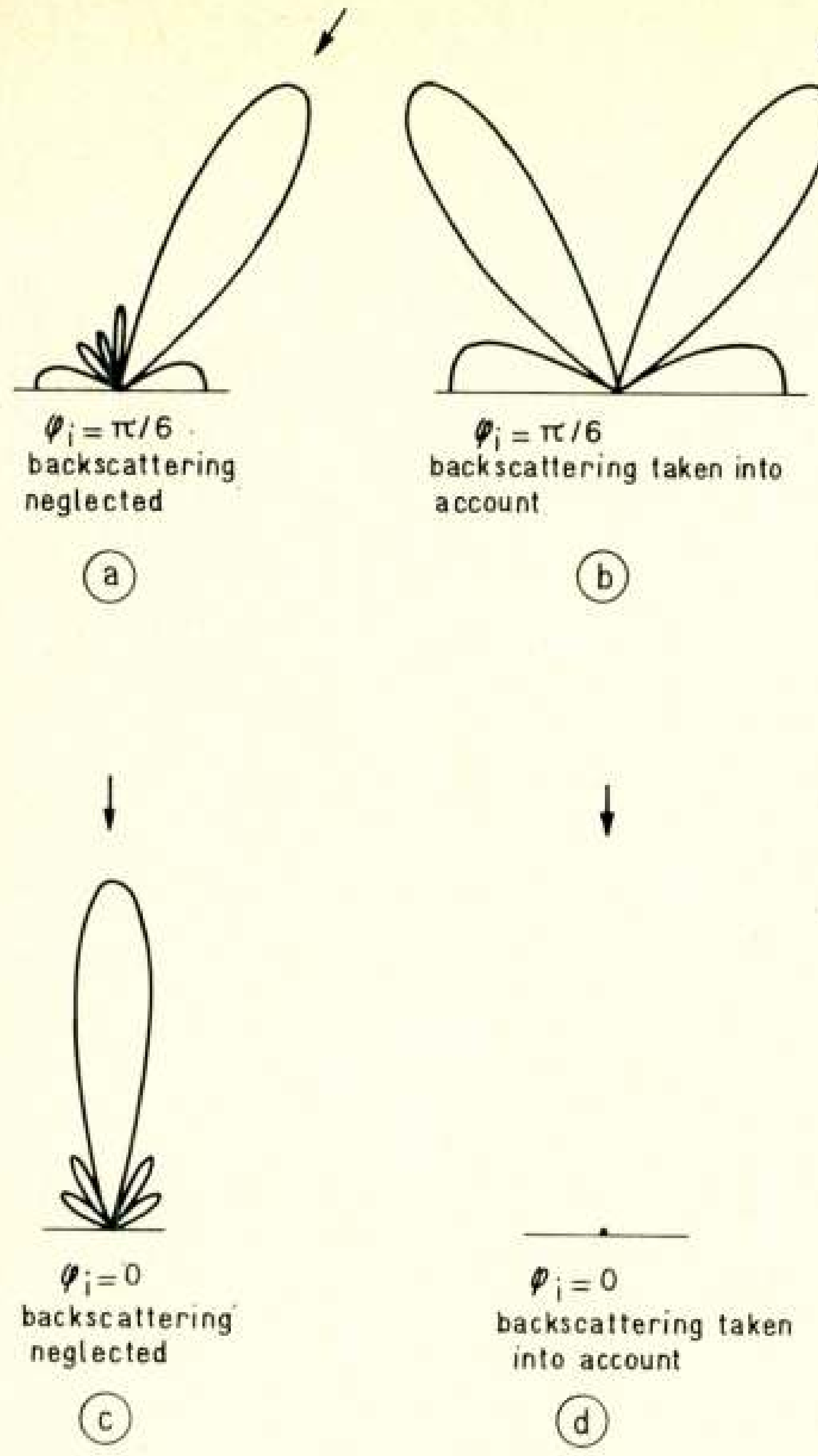


Fig. 6. The reradiation pattern of a passive Van Atta reflector.

electrical lengths of these lines must be the same for all pairs of elements. The operation is as follows (Fig. 4).

Assume an incident plane wave with wavefront L. Power is absorbed by the array elements, transported by the interconnecting lines and reradiated. Now L is also the wavefront of the reradiated wave because the waves reradiated by the elements separately add in phase on L since the electrical pathlengths $A'ADD'$, $B'BCC'$, $C'CBB'$ *and* $D'DAA'$ are equal. This holds independently of array parameters, frequency and angle of arrival.

Fig. 5 shows a variant where the Van Atta array is divided into two subarrays, one for reception and one for transmission to allow the use of unilateral circuit elements in the interconnecting lines. For a review of the proposed applications of the Van Atta reflector in communication and navigation the reader is referred to [7].

Experimental evidence [7] showed however that the above given treatment of the Van Atta reflector is oversimplified. The reason for this is that we did not take into account mutual coupling and scattering effects. Mutual coupling is a crucial point in all kind of antenna arrays. It influences the element match as well as the radiation pattern. In the Van Atta array it can severely disturb the relation between incident and reradiated waves. In practice the effect of mutual coupling can be reduced by choosing sufficiently large element spacings.

Assuming no mutual coupling the effect of scattering by the array elements, while receiving, is still significant. In a Van Atta reflector scattering can violate the Van Atta principle causing radiation in unwanted directions and destructive interference with the desired reradiated wave. From the example of section 3 it can be expected that a Hertzian dipole will be a bad choice as array element in a Van Atta reflector, because the backscattering component of $\underline{E}^d$ has the same strength as the absorbed part of $\underline{E}^c$ which is reradiated according to the Van Atta principle. The same holds for the more practical halfwave dipole [7]. The effect of backscattering is demonstrated in the following example of a passive Van Atta reflector consisting of six equispaced halfwave dipole elements half a wavelength apart. The length of the interconnecting lines is chosen equal to a multiple of the wavelength and perfect match between these lines and the array elements is assumed. Mutual coupling effects are neglected. For plane wave incidence at the angle ($\varphi = \varphi_i; \vartheta = 0$) Fig. 6 shows the reradiation pattern in the XY-plane, with backscattering neglected (a and c) and backscattering taken into account (b and d). Apparently the reflector becomes completely invisible at normal incidence.

To get around the difficulties caused by scattering effects one can use an active Van Atta reflector applying amplification or frequency conversion in the interconnecting lines. Then the interference between backscattering component and Van Atta reradiation may be minimized or eliminated.

References

[1] Montgomery, C. G., Dicke R. H. and Purcell, E. M.: Principles of microwave circuits; Radiation Laboratory Series. Vol. 8 New York: Mc Graw-Hill 1948, pp. 317 ... 333.

[2] Kahn, W. K. and Kurss, H.: Minimum – Scattering Antennas. IEEE transactions on antennas and propagation Vol. AP-13 September 1965, pp. 671 ... 675.

[3] Midgley, D.: A theory of receiving aerials applied to the reradiation of an electromagnetic horn. Proc. IEE Vol. 108B November 1961, pp. 645 ... 650.

[4] Ramo, S. Whinnery J. R. and Duzer, Van T.: Fields and waves in communication electronics. John Wiley and Sons Inc., New York 1965, p. 210.

[5] Montgomery, C. G., Dicke R. H. and Purcell, E. M.: Principles of microwave circuits; Radiation Laboratory Series Vol. 8 New York: Mc Graw-Hill 1948, pp. 146 ... 149.

[6] Van Atta, L. C.: Electromagnetic reflector, U.S. Patent nr. 2908002, serial nr. 514040 October 6, 1959.

[7] Appel – Hansen, J.: The reradiation pattern of a passive Van Atta reflector. Laboratory of Electromagnetic Theory, Technical University of Denmark, Lyngby. March 1966.

*
* *

621.396.677.8

V. Corrugated Conical Horn Antennas with Small Flare Angles

by dr. M. E. J. Jeuken, Department of Electrical Engineering,
Eindhoven University of Technology



Synopsis: In this paper a description is given of the radiation properties of corrugated conical horn antennas with small flare angles. Elsewhere it has been shown by the author that these antennas possess a symmetrical radiation pattern in a relative frequency range 1 : 1.6. This symmetry has been obtained by applying circumferential grooves. If the antenna is given a great length, the radiation patterns become frequency-independent. In that case the shape of the equiphase lines will but slightly depend on frequency. Experimental results confirm the theory.

1. Introduction

A well-known antenna in the microwave region is the parabolic reflector antenna. It consists of a parabolic reflector and a relatively small antenna in the focal region of the reflector. The small antenna is called a feed and the whole configuration is referred to as the focal point system (Fig. 1).

A second possibility is to place the feed in the vicinity of the vertex of the reflector and to apply a hyperbolic reflector in the focal region (Fig. 2). This system is called a Cassegrain antenna, the properties of which have been summarized in [1].

Generally speaking, one may say that Cassegrain antennas are in use as antennas in earth stations for communication with satellites, while the focal point system is used for radio-astronomical investigations. It should be noted that the two systems impose different properties on the feeds. For instance, a feed for a Cassegrain antenna illuminates a small subreflector, while in the focal point system a feed is used which illuminates a rather large reflector. An example of a feed which is used in focal point systems is an open circular waveguide. Sometimes one uses a conical horn antenna with small flare angle and small aperture. This improves the matching of the feed.

It is the purpose of this paper to give a survey of some recent developments with respect to feeds for parabolic reflector antennas.

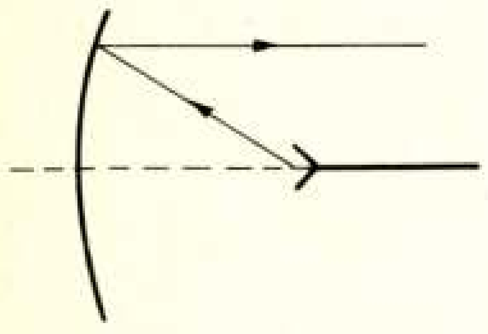


Fig. 1. Diagram of focal point system.

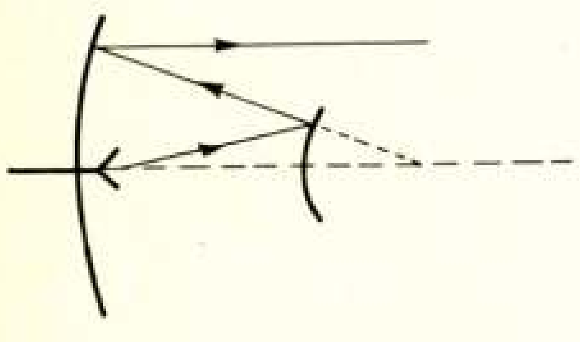


Fig. 2. Diagram of Cassegrain antenna.

2. Conical horn antennas with small flare angles

We shall restrict ourselves to aperture antennas with an aperture S_A as indicated in Fig. 3a. It can be proved that the radial component of the electric field E_r and the corresponding magnetic component H_r are zero in a point P which is at a large distance r from the antenna ($r >> \lambda$, λ is the wavelength in free space). Hence the electric field in P is described by E_θ and E_ϕ, while H_θ and H_ϕ represent the magnetic field. Furthermore, we know that

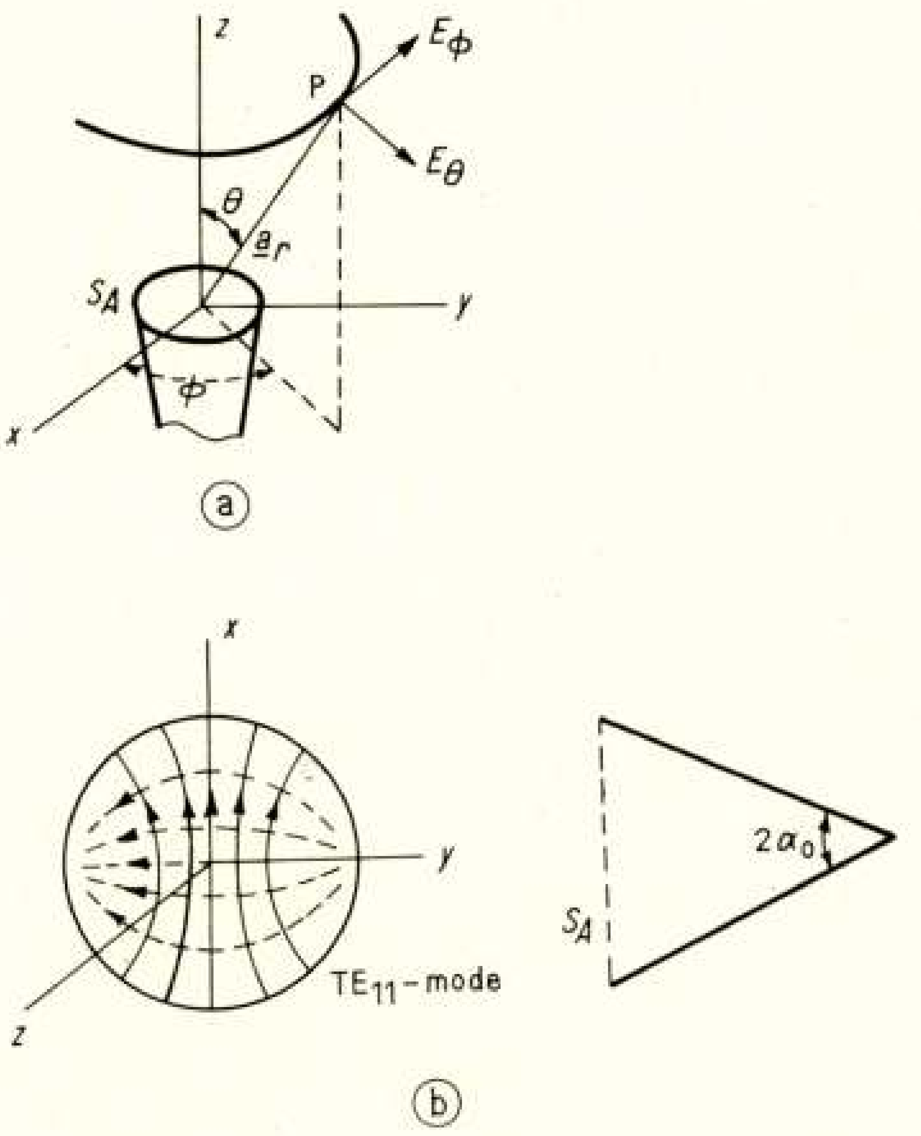


Fig. 3. Aperture, a. co-ordinate system; b. TE_{11}-mode, conical horn antenna.

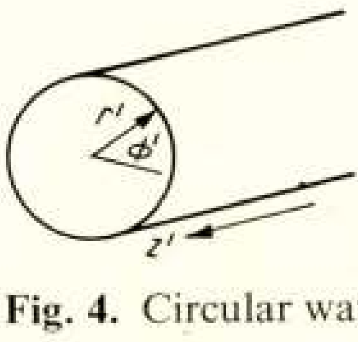


Fig. 4. Circular waveguide.

$$\underline{a}_r \times \underline{E}(\underline{r}) = Z_0 \underline{H}(\underline{r}) \qquad (1)$$

with

$$\underline{a}_r = \frac{r}{r} \text{ and } Z_0 = \sqrt{\frac{\mu_0}{\varepsilon_0}} = 120\pi.$$

Assume that the electromagnetic field in the aperture S_A is known, then we can derive the following expression for the electric field at a point P [2]:

$$\underline{E}(\underline{r}) = \frac{-jk}{4\pi} \frac{e^{-jkr}}{r} \underline{F}(\theta,\varphi) \qquad (2)$$

Here $k = 2\pi/\lambda$ and $\underline{F}(\theta,\phi)$ is a complex vector, which in general is a function of frequency. The function $\exp(-jkr)/r$ represents an outgoing spherical wave because a time-dependence $\exp(j\omega t)$ has been assumed in the derivation of eq. (2).

The next step is that we assume S_A to be the aperture of a conical horn antenna with a small flare angle α_0 and the TE_{11}-mode to be the mode propagated in the horn (Fig. 3b). A further approximation which we shall introduce is that the aperture field is identical with the transverse field of this mode. This field is specified as follows (Fig. 4):

$$\begin{aligned} E_{r'} &= f(r') \cos\phi' \quad Z_0 H_{r'} = \frac{-\beta}{k} g(r') \sin\phi' \\ E_{\varphi'} &= g(r') \sin\phi' \quad Z_0 H_{\varphi'} = \frac{\beta}{k} f(r') \cos\phi' \end{aligned} \qquad (3)$$

β is the propagation constant. The co-ordinates in the aperture are primed, while the co-ordinates of point P mentioned above are unprimed. Now we are able to derive the following expressions for the electric field at a large distance from the antenna:

$$E_\theta(\theta,\varphi) = \frac{+jk}{4\pi} \frac{e^{-jkr}}{r} \cos\varphi \, F_\theta(\theta) \qquad (4)$$

$$E_\phi(\theta,\phi) = \frac{-jk}{4\pi} \frac{e^{-jkr}}{r} \sin\phi \, F_\phi(\theta) \qquad (5)$$

The functions $F_\theta(\theta)$ and $F_\phi(\theta)$ will be found in [3]. For the moment it is important to notice that the functions $F_\theta(\theta)$ and $F_\phi(\theta)$ are not identical.

The x-z plane is the plane characterized by $\phi = 0$. Equations (3) and (4) show that intensity distributions of the radiation in this plane is described by the function $F_\theta(\theta)$. The x-z plane is the E-plane. The y-z plane is the H-plane; the intensity distribution of radiation in this plane is given by $F_\phi(\theta)$. Hence the power radiation pattern is ϕ-dependent and is called non-symmetrical with respect to the antenna-axis (z axis). To illustrate this property, we measured the power radiation pattern of a conical horn antenna with small flare angle, having the TE_{11}-mode propagated in this antenna. The measurements were carried out for 7.6 GHz in the E-plane and the H-plane [4]. The results are given in Fig. 5; and it may be observed that the patterns in the two planes are not identical. We also measured the radiation patterns at 11.4 GHz. The diagrams for this frequency are given in Fig. 6 and it may be seen that the beamwidth is smaller. In conclusion we may say that the pattern of a conical horn antenna with small flare angle is asymmetric and frequency-dependent.

In the following sections we shall discuss a method for obtaining symmetrical patterns and in the last section it will be shown how patterns can be obtained which are independent of frequency in a rather large frequency band and which are nearly symmetrical in that band.

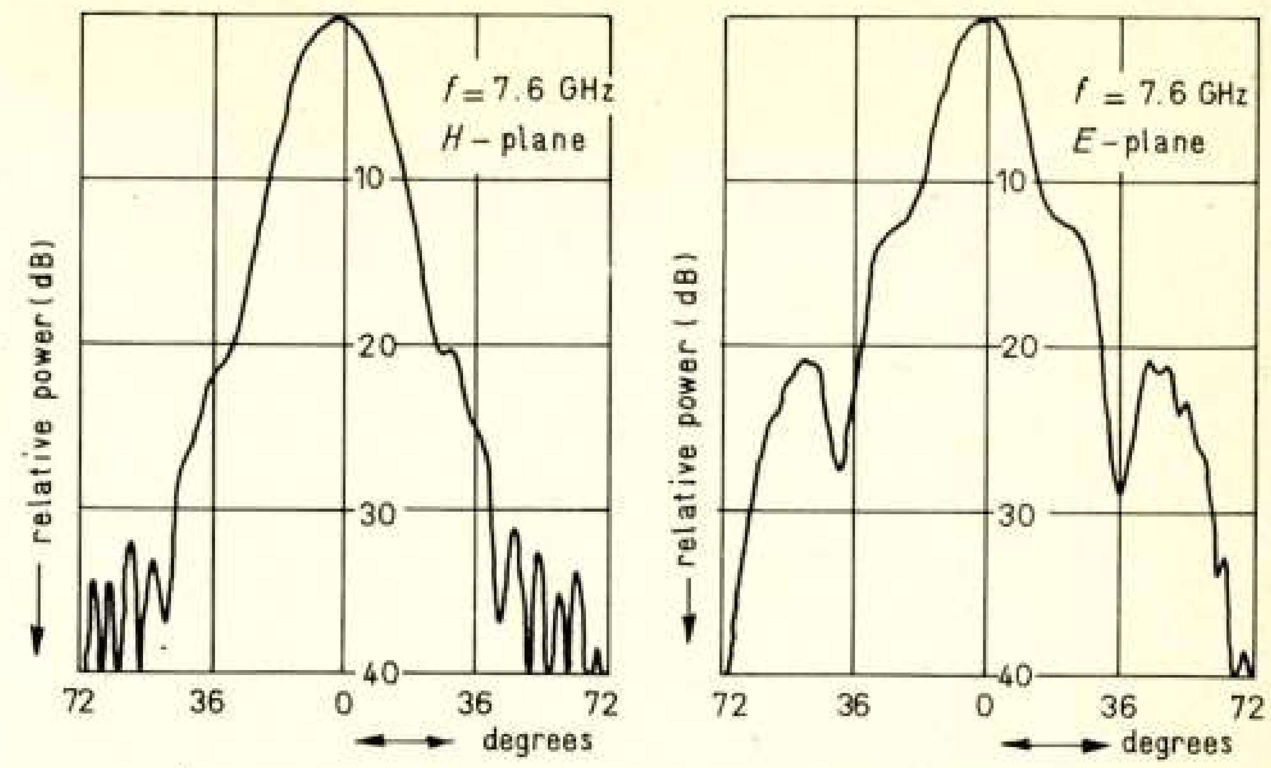


Fig. 5. Power radiation pattern of conical horn antenna with small flare angle.

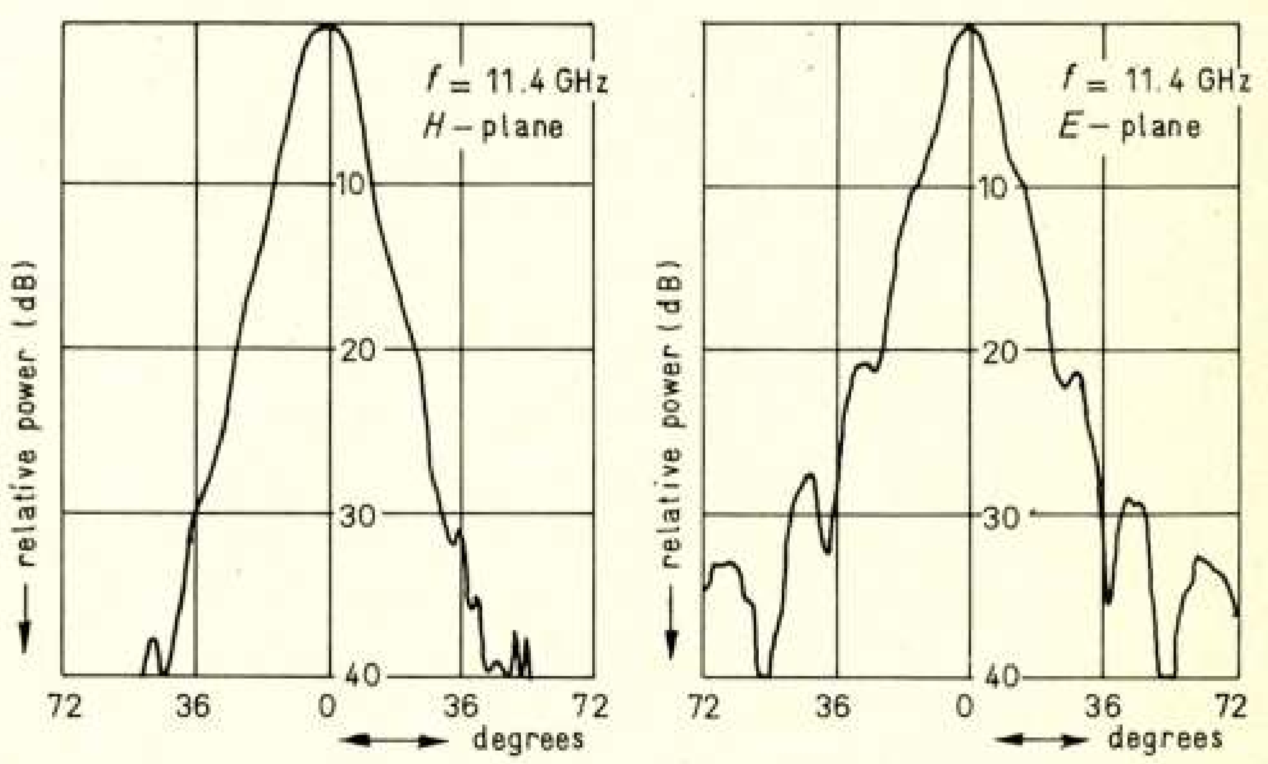


Fig. 6. Power radiation pattern of conical horn antenna with small flare angle.

3. Symmetrical radiation pattern

It is possible to specify electromagnetic fields in the aperture S_A of the antenna that give rise to a symmetrical radiation pattern. The fields are [3]:

$$\begin{aligned} E_{r'} &= f'(r') \cos\phi' \qquad Z_0 H_{r'} = f'(r') \sin\phi' \\ E_\phi' &= g'(r') \sin\phi' \qquad Z_0 H_{\phi'} = -g'(r') \cos\phi' \end{aligned} \qquad (6)$$

It should be noted that in eq. (6) the r'-dependence of $E_{r'}$ and $Z_0 H_{r'}$ is described by the same function. An analogous observation can be made with respect to the components $E_{\phi'}$ and $Z_0 H_{\phi'}$.

Inspection of eq. (3) shows that for the TE_{11}-mode $E_{r'}$ and $Z_0 H_{\phi'}$ depend equally on r' and the same can be said about $E_{\phi'}$ and $Z_0 H_{r'}$. Substitution [2] of eq. (6) in $\underline{F}(\theta,\phi)$ of eq. (2) gives after some mathematics

$$\begin{aligned} E_\theta &= F(\theta) \cos\phi \\ E_\phi &= -F(\theta) \sin\phi \end{aligned} \qquad (7)$$

The time-average Pointing vector is

$$\underline{P} = \tfrac{1}{2} \mathrm{Re}\,[\underline{E} \times \underline{H}^*] = \frac{1}{2Z_0} \{|E_\theta|^2 + |E_\phi|^2\}\, \underline{a}_r = \frac{1}{2Z_0} |F(\theta)|^2 \underline{a}_r \qquad (8)$$

In the derivation of eq. (8) use has been made of eq. (1) and we notice that $\underline{P}$ is independent of ϕ, which implies that the power radiation is symmetrical.

The next task is to investigate whether the fields given in eq. (6) can berealized. One can prove that the fields of eq. (6) cannot be obtained as transverse fields in a circular waveguide with a perfectly conducting boundary. The proof is as follows. Owing to the perfectly conducting boundary, $E_{z'}$ and $E_{\phi'}$ are zero at that boundary. Then the normal component of the magnetic field is also zero [5].

Hence, $H_{r'}$ is zero at the boundary and $E_{r'}$ is also zero owing to the special character of the field specified in eq. (6). Hence we know that the vector $\underline{H} = H_{\phi'} \underline{i}_\phi + H_{z'} \underline{i}_z$ is zero. So there exist no currents or charges on the boundary of the waveguide, and fields of the type described in eq. (6) cannot exist.

Suppose that we try to design a circular waveguide in which modes can exist, composed of a transverse electric field and a transverse magnetic field as specified in eq. (6). From the divergence equations we derive that these modes have $E_{z'}$ and $H_{z'}$ components, which in general have values differing from zero. We shall prove here that these modes can exist in a circular waveguide with a very special anisotropic boundary. This boundary is characterized by the conditions

$$E_{z'} = Z_{z'} H_{\phi'} \qquad (9)$$

$$E_{\phi'} = Z_{\phi'} H_{z'}$$

with the special conditions $Z_{\phi'} = 0$ and $Z_{z'} = \infty$.

These conditions imply that

$$E_{\phi'} = 0 \qquad Z_0 H_{\phi'} = 0 \qquad (10)$$

$$E_{z'} \neq 0 \qquad Z_0 H_{z'} \neq 0$$

at the boundary.

A solution of Maxwell's equations satisfying the above boundary conditions can be the sum of a TE- and a TM-field [3], [6]. The result in the co-ordinates of Fig. 4 is:

$$E_{r'} = \left[-\frac{n}{r'} \mathrm{J}_n(k_c r') - \frac{\gamma}{\mathrm{j}k} k_c \alpha \mathrm{J}_n'(k_c r') \right] \cos n\varphi' \qquad (11)$$

$$E_{\varphi}' = \left[k_c \mathrm{J}_n'(k_c r') + \frac{\gamma}{\mathrm{j}k} \alpha \frac{n}{r'} \mathrm{J}_n(k_c r') \right] \sin n\phi' \qquad (12)$$

$$Z_0 H_{r'} = \left[\frac{-\gamma}{\mathrm{j}k} k_c \mathrm{J}_n'(k_c r') - \alpha \frac{n}{r'} \mathrm{J}_n(k_c r') \right] \sin n\phi' \qquad (13)$$

$$Z_0 H_{\varphi'} = \left[\frac{-\gamma}{\mathrm{j}k} \frac{n}{r'} \mathrm{J}_n(k_c r') - \alpha k_c \mathrm{J}_n'(k_c r') \right] \cos n\phi' \qquad (14)$$

$$E_{z'} = \frac{k_c^2}{\mathrm{j}\omega\mu_0} Z_0 \alpha \mathrm{J}_n(k_c r') \cos n\phi' \qquad (15)$$

$$Z_0 H_{z'} = \frac{k_c^2}{\mathrm{j}\omega\mu_0} Z_0 \mathrm{J}_n(k_c r') \sin n\phi' \qquad (16)$$

with $k_c^2 = k^2 + \gamma^2$. The prime denotes differentiating with respect to $k_c r'$. In these expressions the factor $\exp(\mathrm{j}\omega t - \gamma z)$ has been omitted. The choice $n = 1$ and $\alpha = 1$ gives rise to transverse fields which are of the type specified in eq. (6). The dispersion equation can be derived after introducing the boundary conditions of eq. (10):

$$k_c \mathrm{J}_1'(k_c a) + \frac{\gamma}{\mathrm{j}k} \frac{1}{a} \mathrm{J}_1(k_c a) = 0, \qquad (17)$$

where a is the radius of the circular waveguide.

It should be noted that the choice $\alpha = -1$ gives rise to transverse fields, which, used as aperture fields, produce a symmetrical radiation pattern as well. However, in this case the radiation pattern has a dip for $\theta = 0$ [7]. So this mode is not suitable for antenna applications. The modes given in eqs. (11) to (16) incl. are hybrid modes ($E_{z'} \neq 0$ and $H_{z'} \neq 0$). The modes associated with $\alpha = 1$ are $\mathrm{HE}_{nm}^{(1)}$-modes and those associated with $\alpha = -1$ are $\mathrm{HE}_{nm}^{(2)}$-modes.

The dispersion equation for $\mathrm{HE}_{nm}^{(2)}$-modes can easily be found. The result is

$$k_c \mathrm{J}_1'(k_c a) - \frac{\gamma}{\mathrm{j}k} \frac{1}{a} \mathrm{J}_1(k_c a) = 0. \qquad (18)$$

For the propagating modes $\gamma = \mathrm{j}\beta$. The solution of eq. (17) and eq. (18) is plotted in Fig. 7, and we observe that the $\mathrm{HE}_{11}^{(1)}$-mode

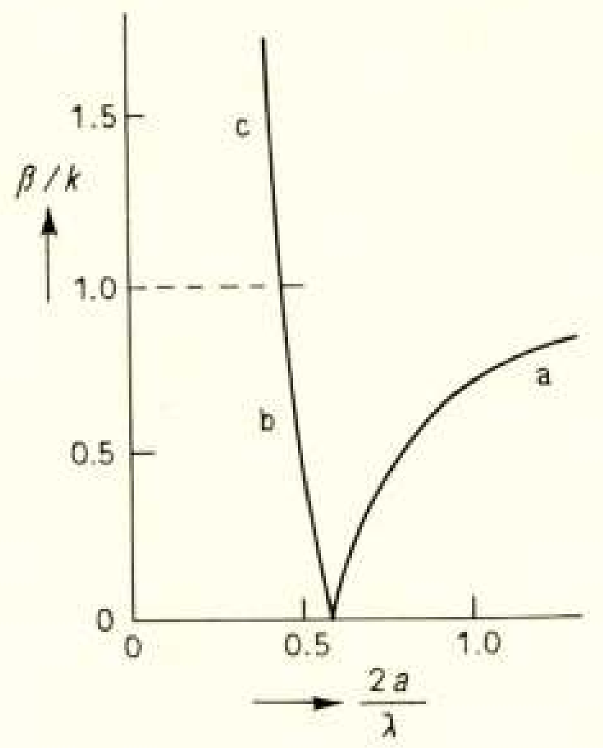


Fig. 7. $\frac{\beta}{k}$ against $\frac{2a}{\lambda}$ for circular waveguide with anisotropic boundary:
a: $\mathrm{HE}_{11}^{(1)}$-mode;
b: fast $\mathrm{HE}_{11}^{(2)}$-mode;
c: slow $\mathrm{HE}_{11}^{(2)}$-mode.

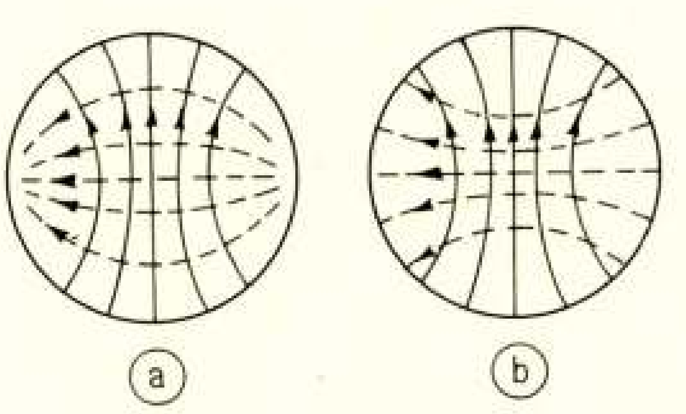


Fig. 8. Transverse electric and transverse magnetic field lines:
a: TE_{11}-mode;
b: $\mathrm{HE}_{11}^{(1)}$-mode for $\frac{2a}{\lambda} = 0.6$.

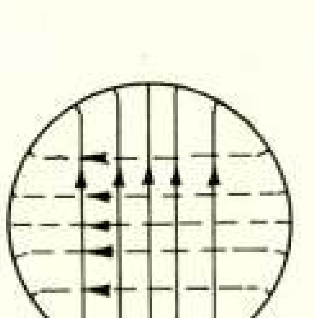


Fig. 9. Transverse electric and transverse magnetic field lines of the $\mathrm{HE}_{11}^{(1)}$-mode for large values of $\frac{2a}{\lambda}$

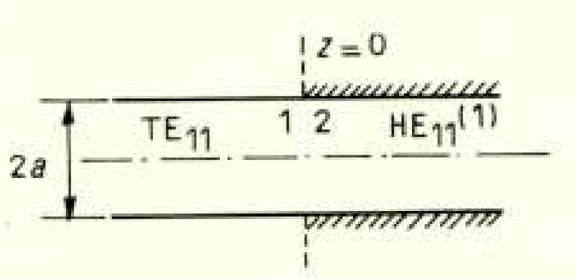


Fig. 10. Transition from a perfectly conducting waveguide to a waveguide with anisotropic boundary.

is a fast wave, while the other is fast or slow depending on $\frac{2a}{\lambda}$.
The $HE_{11}^{(1)}$-mode can propagate, provided that $\frac{2a}{\lambda} > 0.58$. This condition is the same as that for which the TE_{11}-mode can propagate in a circular waveguide with a perfectly conducting boundary. The field lines of the $HE_{11}^{(1)}$-mode and the TE_{11}-mode are plotted in Fig. 8 for $\frac{2a}{\lambda} = 0.6$. It should be noted that the shape of the field lines of the TE_{11}-mode is independent of $\frac{2a}{\lambda}$. However, the field lines of the $HE_{11}^{(1)}$-mode become straight lines for large values of $\frac{2a}{\lambda}$. (Fig. 9).

One will now understand how the $HE_{11}^{(1)}$-mode can be generated. By coupling a perfectly conducting circular waveguide to a circular waveguide, for which the boundary conditions given in eq. (9) are valid, one is able to excite the $HE_{11}^{(1)}$-mode, provided the TE_{11}-mode propagates in the circular waveguide with perfectly conducting boundary (Fig. 10). Owing to the fact, that the $HE_{11}^{(1)}$- and TE_{11}-modes have the same cut-off frequency, the $HE_{11}^{(2)}$-mode cannot be excited. The field lines of the $HE_{11}^{(1)}$-mode are similar to those of the TE_{11}-mode. Hence, the $HE_{11}^{(1)}$-mode will be excited with high effiency. Calculations concerning this question can be found in the literature [7].

Our next task is to compute the radiation pattern of an open radiating circular waveguide with the anisotropic boundary described in eq. (9). The calculations will be found in [3] and the results are plotted in Fig. 11. The conclusion is that te pattern is symmetrical. The beamwidth of the pattern is a function of $\frac{2a}{\lambda}$. This well-known phenomenon has also been found for an open radiating circular waveguide with a perfectly conducting boundary.

4. The corrugated waveguide

In this section we shall prove that a circular waveguide with boundary conditions as specified in eq. (9) is a corrugated waveguide (Fig. 12). Such a waveguide consists of a central part (I) and equally spaced grooves (II). It is a periodic structure; an exact theory describing it should start by the writing down of the electromagnetic field in the central part in the form of a series of space harmonics. The next step will then be to find the electromagnetic fields in the grooves. After introducing the boundary conditions at $r' = a$, an equation for the propagation constant β is obtained. In our case the distance between two consecutive grooves is so short that a great number of grooves

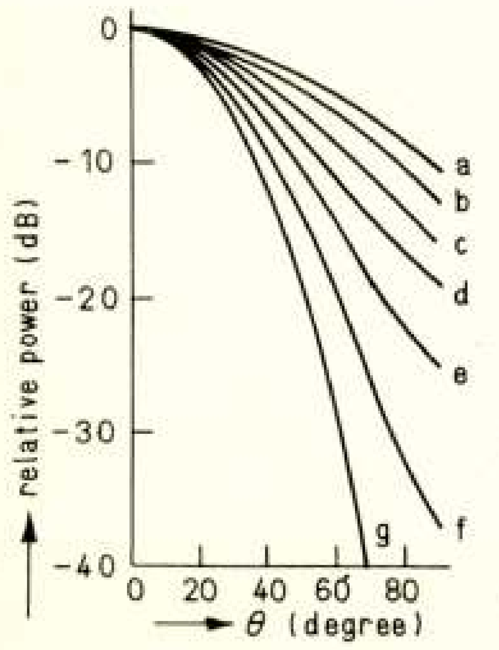


Fig. 11. Power radiation pattern of a radiating circular waveguide with anisotropic boundary.

a: $\frac{2a}{\lambda} = 0.6$ b: $\frac{2a}{\lambda} = 0.8$ c: $\frac{2a}{\lambda} = 1.0$

d: $\frac{2a}{\lambda} = 1.2$ e: $\frac{2a}{\lambda} 1.4$ f: $\frac{2a}{\lambda} = 1.6$

g: $\frac{2a}{\lambda} = 1.8$.

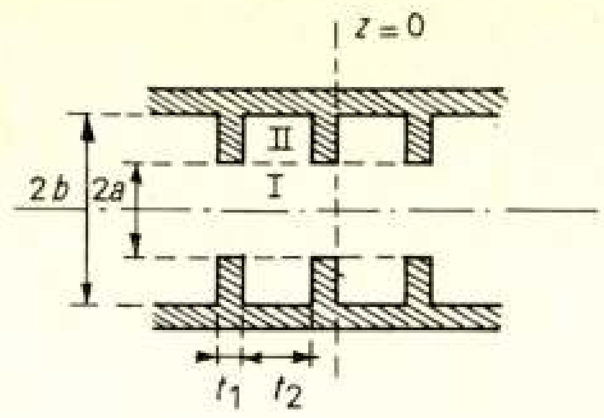


Fig. 12. Circular corrugated waveguide.

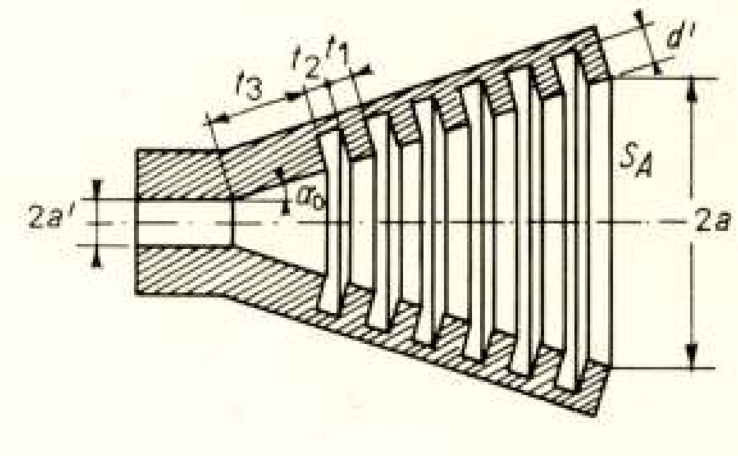


Fig. 13. Corrugated conical horn antenna.

are present per wavelength, and we thus are able to formulate average boundary conditions. A detailed study of the electromagnetic fields which can exist in a groove is given in [3]. The main conclusion is as follows. If the width t_2 of the groove is smaller than half a wavelength, only one class of modes can propagate in the r' direction. This class of modes consists of modes with different ϕ' dependence. Which of these modes will be excited is determined by the electromagnetic field in the central part (I). The modes mentioned above have the following components: $E_{z'}$, $H_{r'}$, and $H_{\phi'}$. Hence $E_{\phi'} = 0$ at the open part of the groove (we neglect higher evanescent modes). Of course, $E_{\phi'}$ is also zero on the dams between two grooves.

Furthermore, we assume that the width of the dams is infinitely small. On the dams only a current in the ϕ' direction is possible. A component $H_{z'}$ accompanies this current. The modes with the components $E_{z'}$, $H_{r'}$ and $H_{\phi'}$ propagate in the radial direction and reflect on the perfectly conducting boundary at $r' = b$. If the depth of the groove is a quarter of a wavelength, then we know that H_{ϕ} is zero at the opening of the groove. Hence the corrugated waveguide is a structure with boundary conditions specified in the set of eq. (9). However, this is true for only one frequency. The next step would be to investigate the corrugated waveguide at other frequencies. However, this task is beyond the scope of the present paper. The relevant information can be found in [7] and [8].

5. The corrugated conical horn antenna with small flare angle

In section 3 we have discussed the radiation pattern of an open radiating circular waveguide with the anisotropic boundary described by eq. (9). In this section we shall present some results of theoretical and experimental work on corrugated conical horn antennas with small flare angles (Fig. 13). The flare angle $\alpha_0 \leq 15°$. This offers the possibility of treating the antenna as a circular waveguide radiator. At first we calculated the transverse fields in a corrugated waveguide with a diameter equal to that of the aperture of the antenna. The influence of the depth of the grooves has been taken into account in this calculation.

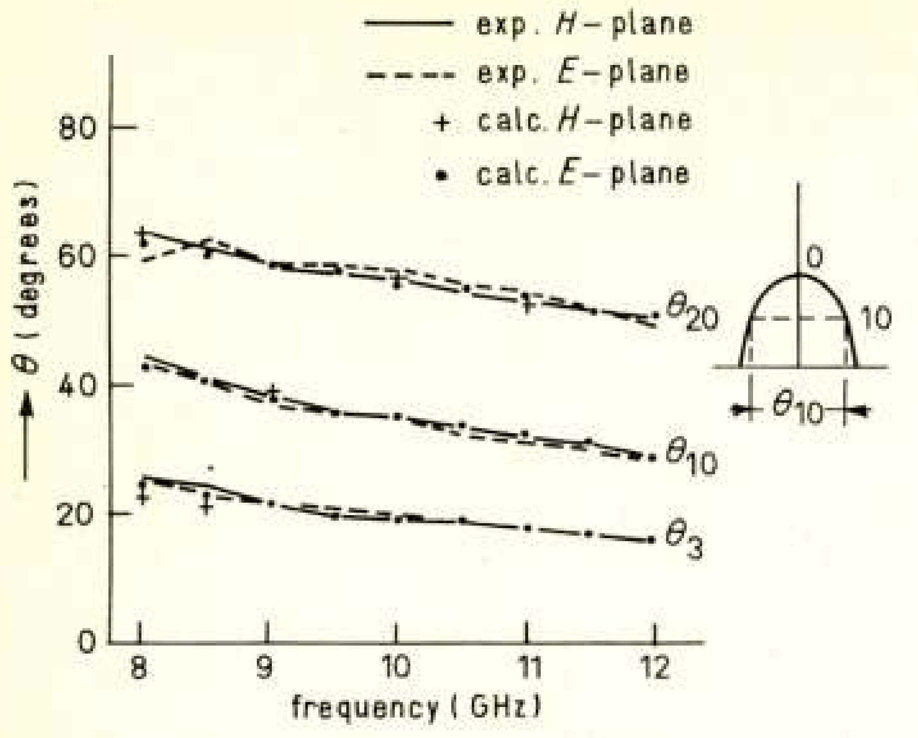


Fig. 14. Beamwidth against frequency; $\alpha_o = 15°$, $2a = 91$ mm, $d' = 9$ mm.

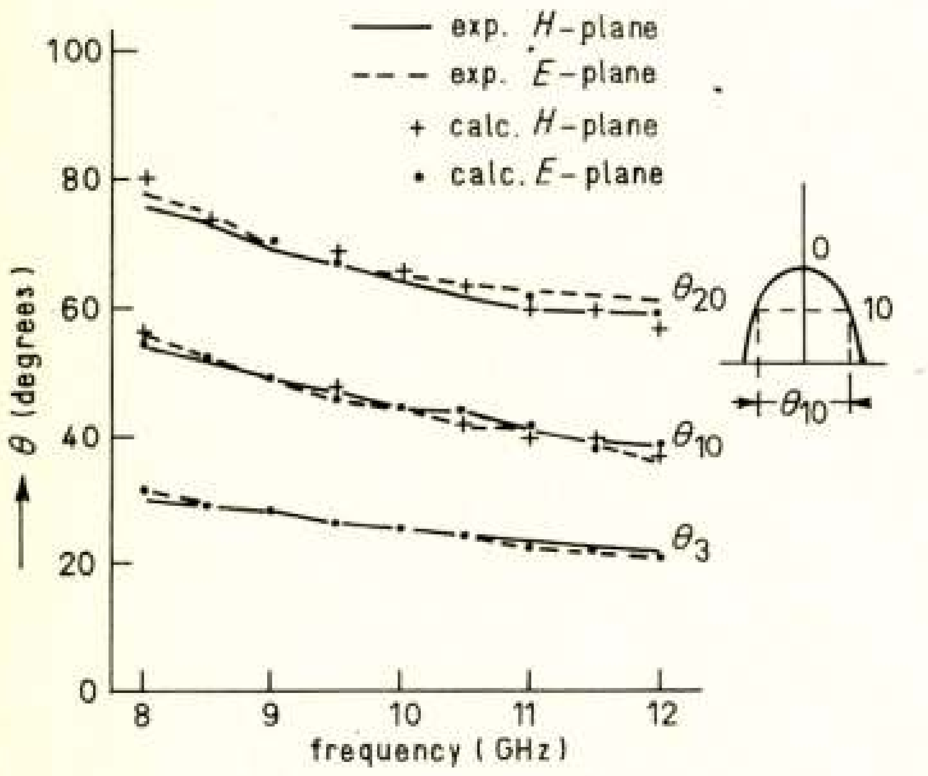


Fig. 15. Beamwidth against frequency; $\alpha_o = 15°$, $2a = 121$ mm, $d' = 9$ mm.

The transverse fields which were found in this way have been substituted in formulae giving the radiation pattern [8]. The result is similar to that of the eqs. (4) and (5). For the special case that $H_\phi = 0$ it is found that the pattern is symmetrical.

The radiation pattern of two antennas has been investigated both theoretically and experimentally by using the forementioned procedure. The results are plotted in Figs. 14 and 15. A rather good agreement was found to exist between theoretical and experimental results. A second conclusion is that the pattern is symmetrical not only for the frequency for which $H_{\phi'} = 0$, but also for a wide frequency range above that frequency. The third conclusion is that the beamwidth varies only slightly as a function of frequency. The largest antenna exhibits this effect to a greater extent. It should be observed that this phenomenon is in contrast with the results obtained in section 3, where the radiation pattern of an open radiating waveguide with the boundary condition described by eq. (9) was discussed. Similar results have been reported by Clarricoats and Saha [7]. The phenomenon that the radiation patterns of the two antennas are more or less independent of frequency is very interesting, because it thus seems possible to design frequency-independent antennas which, moreover, possess symmetrical patterns. It would appear that this frequency-independence is caused by the fact that the aperture is not an equiphase plane, but that a phase distribution across the aperture exists which is a quadratic function of the radius sector in the aperture (Fig. 16). The phase distribution across the aperture is $\exp - j\left[kd\left(\frac{r'}{a}\right)^2\right]$. It will be shown in the next section that frequency-independent and symmetrical patterns can be obtained provided the dimensions of the antenna are chosen properly.

6. Broadband corrugated conical horn antennas with small flare angles

The conclusion of the previous section is that for the microwave region perhaps broadband antennas can be realized having a symmetrical radiation pattern. It seems that corrugated conical horn antennas with proper phase distribution across the aperture give rise to frequency-independent properties. A heuristic consideration concerning this question is given elsewhere [3]. The main conclusion is that d (Fig. 16) should be about half a wavelength for frequencies in the centre of the frequency band. Using this information, the radiation pattern has been calculated of a corrugated conical horn antenna of great length, with a flare angle $\alpha = 15°$. The dimensions of the antenna are given in Table 1. In Fig. 17 the results of a theoretical study are plotted; it will be noticed that a broadband horn antenna with a symmetrical pattern can be designed [9]. Fig. 18 gives an example of the radiation pattern for 8,3 GHz.

Table 1. Dimensions of the antenna, sketched in Fig. 13.

$2a$ [mm]	$2a'$ [mm]	α_o	d' [mm]	t_1 [mm]	t_2 [mm]	t_3 [mm]
264	28	15°	9	3.8	2.3	7

In Fig. 19 experimental results are collected and these are compared with the theoretical results. Agreement is reasonably good, especially for frequencies just above that for which $H_{\phi'} = 0$ at the open part of the grooves. The matching of the antenna has been studied experimentally and the results are shown in Fig. 20. Unfortunately, the V.S.W.R. is high at the lower limit of the frequency range. However, techniques are available to improve the matching [10].

The broadband antenna discussed above is very suitable as a feed in a Cassegrain antenna. In this case it is necessary for the equiphase surfaces to be spheres. A less stringent requirement is that the shape of the equiphase surfaces is independent of frequency. Here, shaped reflectors can be used in the Cassegrain system [4]. The electric field in the far field region of the antenna of Table 1 is given in [3], [8].

$$E_\theta(\theta,\phi) = \frac{jk}{4\pi}\frac{e^{-jkr}}{r}\cos\phi\; F_\theta(\theta,\, kd)$$

$$E_\phi(\theta,\phi) = -\frac{jk}{4\pi}\frac{e^{-jkr}}{r}\sin\phi\; F_\phi(\theta,\, kd) \qquad (19)$$

The pattern is now a function of kd. Let us assume for the moment that $F_\theta(\theta,kd)$ and $F_\phi(\theta,kd)$ are real functions. The distance form the observation point to the centre of the aperture S_A of the antenna is r. Hence the spheres with a centre coinciding with the centre of the aperture, and having a radius r, are

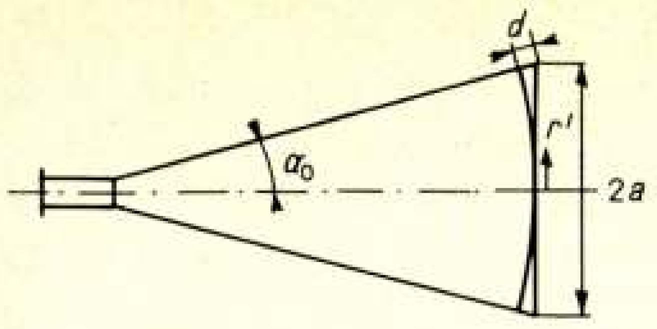


Fig. 16. Diagram or the conical horn antenna.

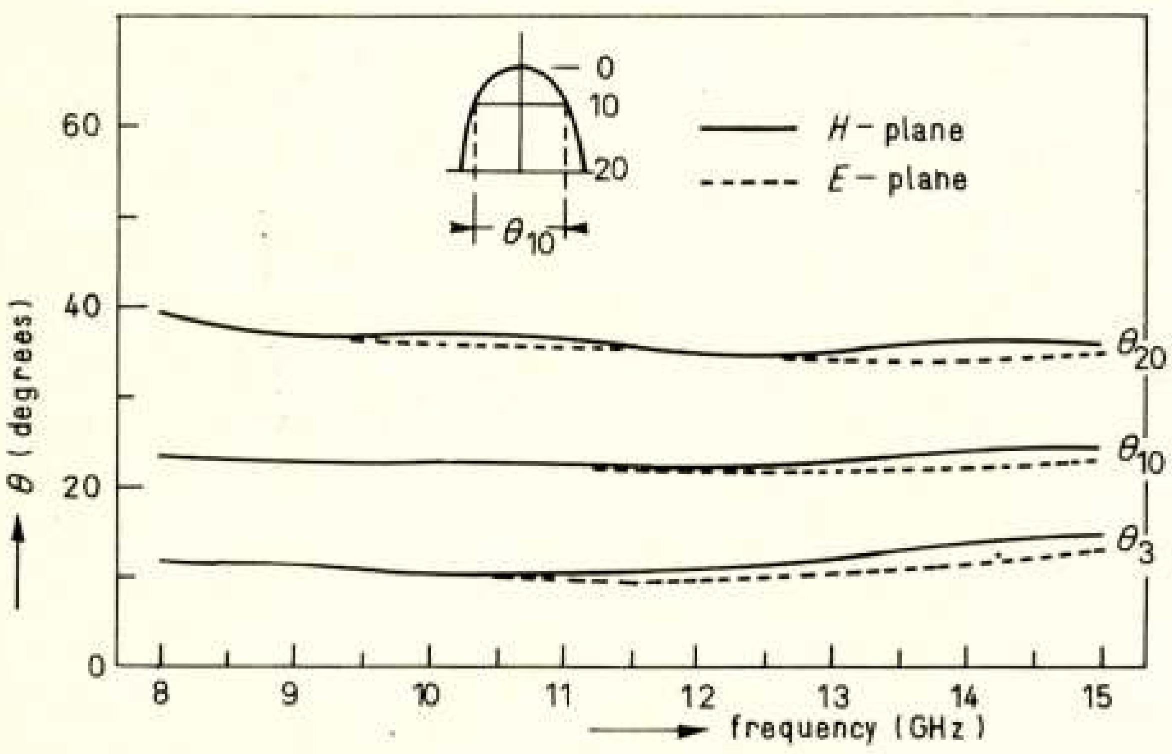


Fig. 17. Beamwidth against frequency; calculated.

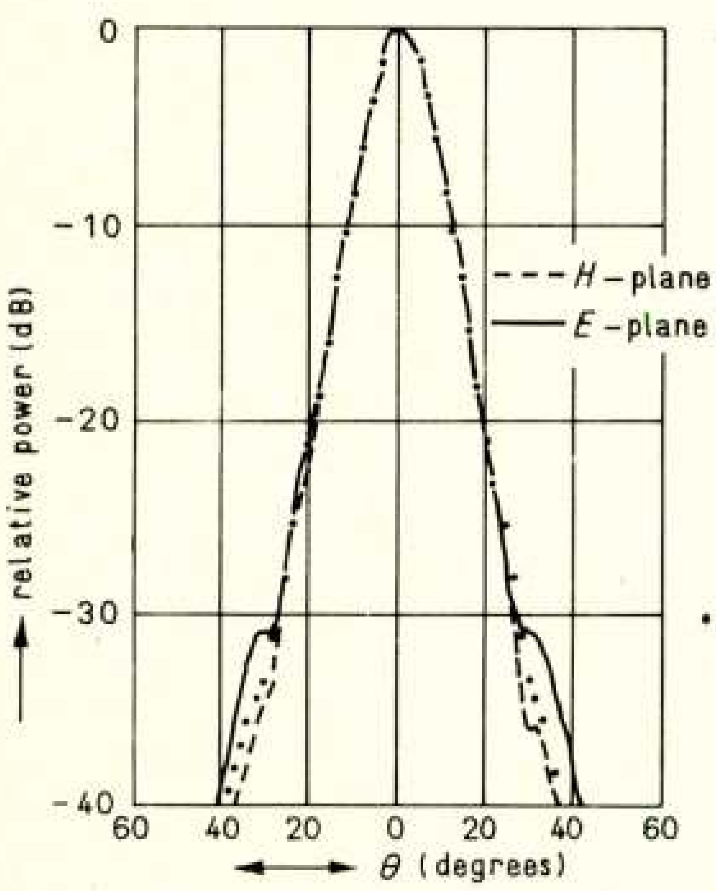


Fig. 18. Power radiation pattern at 8.3 GHz.

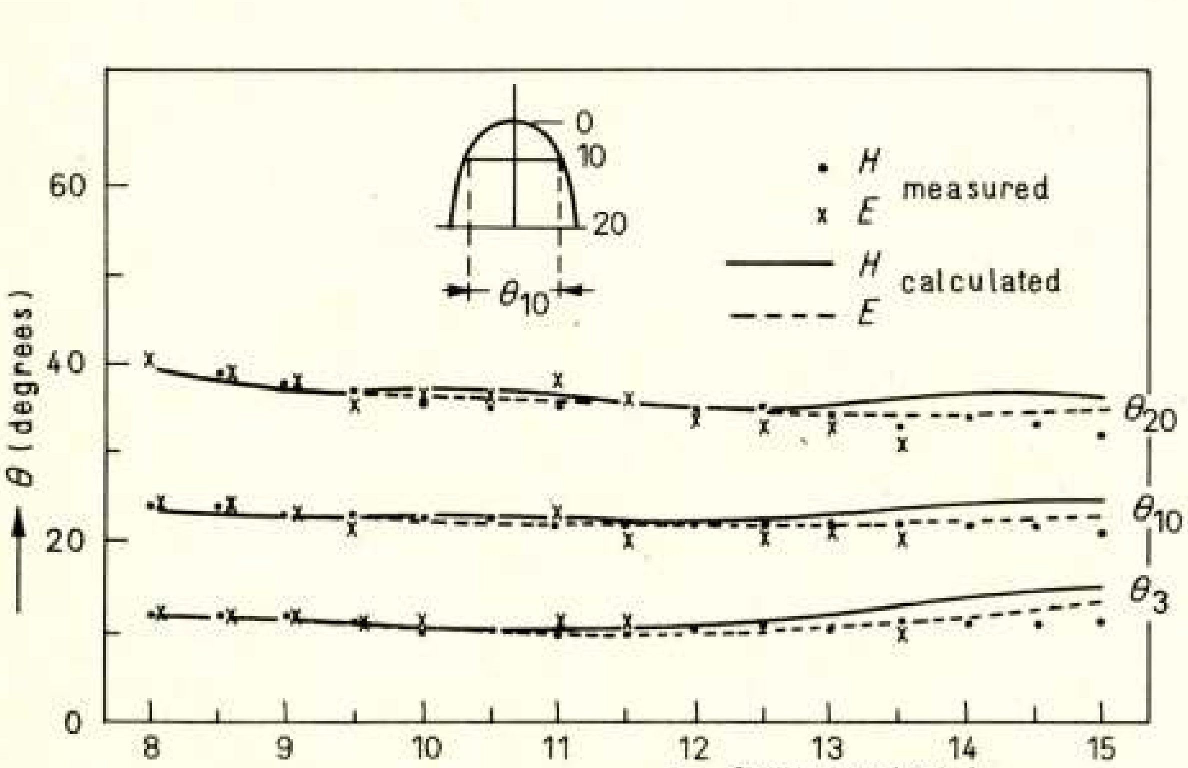


Fig. 19. Beamwidth against frequency; measured.

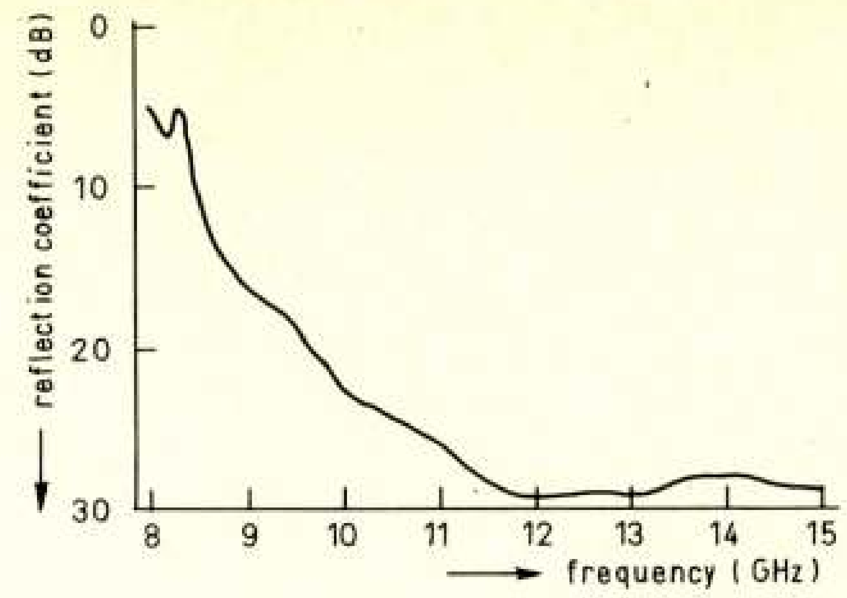


Fig. 20. Reflection coefficient against frequency.

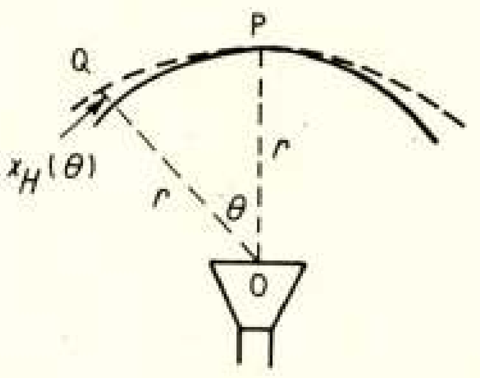


Fig. 21. Horn antenna and equiphase line PQ in far field region.

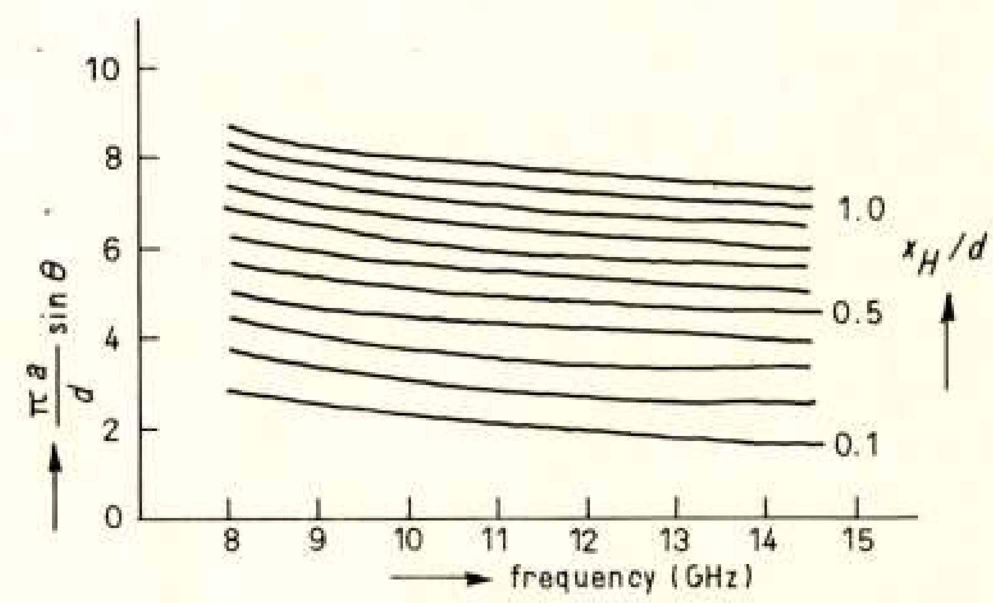


Fig. 22. Curves of constant $\frac{\varkappa_H(\theta)}{d}$-value against $\frac{d}{\lambda}$ of corrugated conical horn of Table 1.

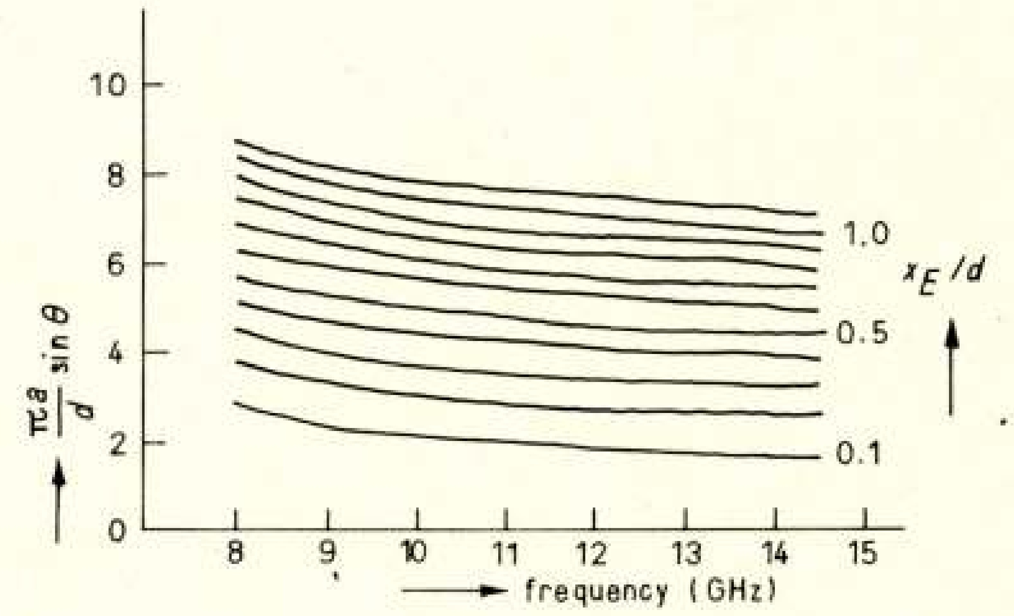


Fig. 23. Curves of constant $\frac{\varkappa_E(\theta)}{d}$-value against $\frac{d}{\lambda}$ of corrugated conical horn of Table 1.

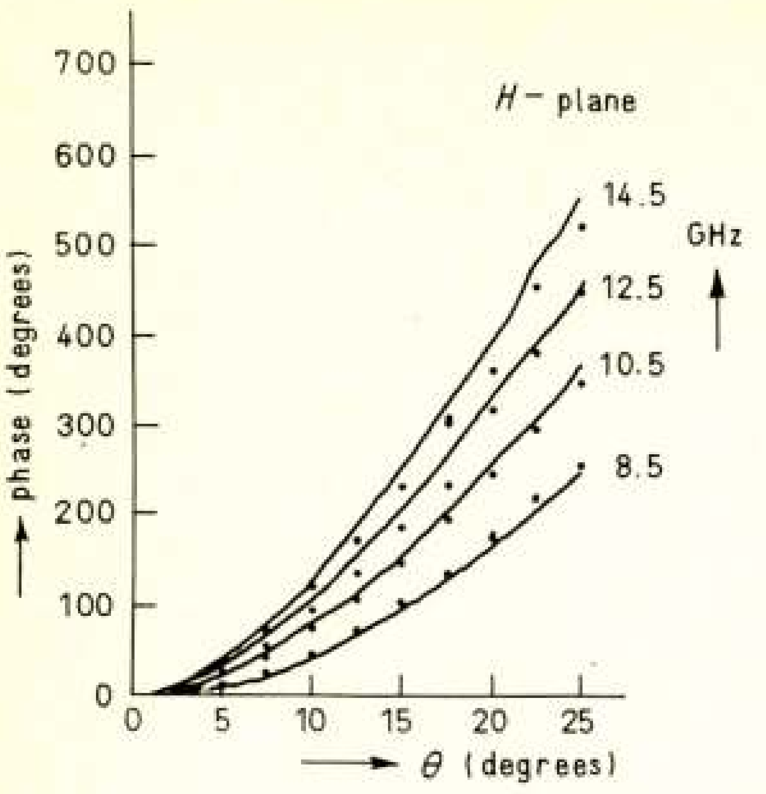


Fig. 24. Measured phase variations in H-plane of the corrugated conical horn of Table 1.

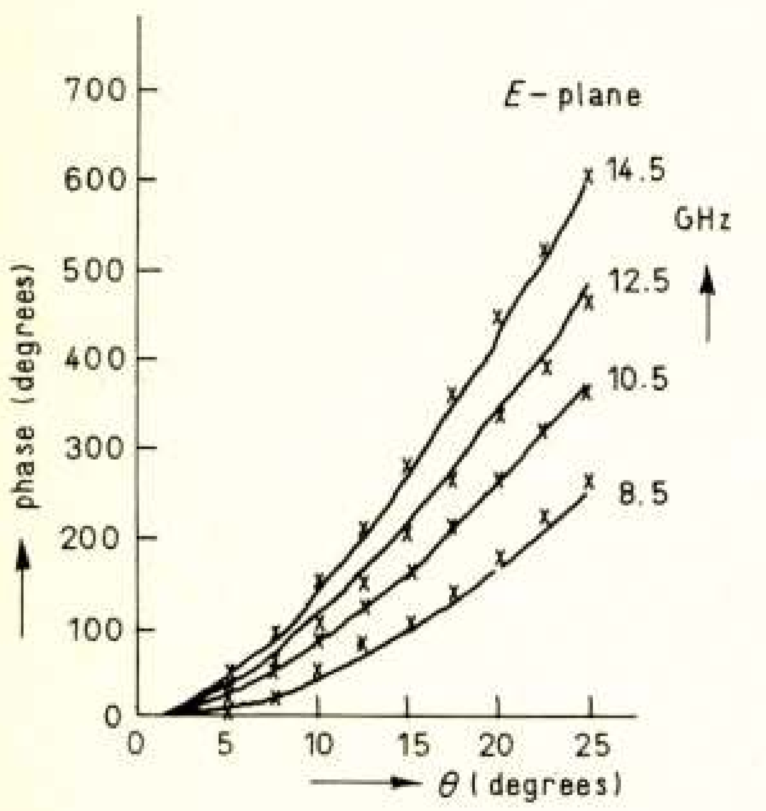


Fig. 25. Measured phase variations in E-plane of the corrugated conical horn of Table 1.

equiphase surfaces. However, in general both $F_\theta(\theta,kd)$ and $F_\phi(\theta,kd)$ are complex functions and we write:

$$F_\theta(\theta,kd) = |F_\theta(\theta,kd)|\, e^{j\psi_E(\theta,kd)}$$
$$F_\varphi(\theta,kd) = |F_\phi(\theta,kd)|\, e^{j\psi_H(\theta,kd)} \quad (20)$$

The physical interpretation of the functions $\psi_E(\theta,kd)$ and $\psi_H(\theta,kd)$ is as follows (Fig. 21). PQ is an equiphase line in the H-plane. The solid line is an arc of a circle, the centre of which coincides with the centre of the aperture S_A.
The function

$$x_H(\theta,kd) = \frac{\lambda}{2\pi}\left[\psi_H(\theta,kd) - \psi_H(\theta,kd)\right] \quad (21)$$

offers the possibility to construct equiphase lines (Fig. 21). The functions $x_H(\theta)$ and $x_E(\theta)$ have been calculated for the antenna of Table 1. This information has been collected in Fig. 22 and Fig. 23. If the curves in Figs. 22 and 23 were straight lines parallel to the frequency axis, then we would conclude that the shape of the equiphase lines in H-plane and E-plane are frequency-independent. However, we observe a slight frequency dependence, but the shape of the equiphase lines is identical in the H-plane and E-plane. In order to verify the theoretical results of Figs. 22 and 23, we measured $x_H(\theta)$ and $x_E(\theta)$. The measuring method is described in [3] and the results of the measurements are plotted in Figs. 24 en 25. We observed a rather good agreement between experimental and theoretical results, especially at 10.5 GHz and 12.5 GHz.

7. Conclusions

In this paper the radiation properties of corrugated conical horn antennas with small flare angles have been treated. These antennas possess a symmetrical radiation pattern if $H_{\phi'} = 0$ at the opening of the grooves. The pattern remains virtually symmetrical in a frequency range 1:1.6. The condition $H_{\phi'} = 0$ at the open part of the grooves determines the lower frequency. The beamwidth is a function of frequency. The beamwidth gets smaller with increasing frequency. If the length of the antenna is chosen such that a quadratic phase distribution exists across the aperture, then frequency-independent patterns are obtained in a frequency range 1:1.6. The study of the equiphase lines shows that the shape of these lines depends but slightly on frequency. Experimental results confirm the theory.

References

[1] DIJK, J., JEUKEN, M. E. J. and MAANDERS E. J.: 'Blocking and diffraction in Cassegrain antenna systems', De Ingenieur, 5 juli 1968, blz. 097 ... 091.
[2] JEUKEN, M. E. J. and KIKKERT, J. S.: 'A broadband aperture antenna with a narrow beam', Alta Frequenza, 38, 1969, pp. 270 ... 276.
[3] JEUKEN, M. E. J.: 'Frequency-independence and symmetry properties of corrugated conical horn antennas with small flare angles', Thesis, 1970, Eindhoven University of Technology.
[4] DIJK, J., JEUKEN, M. E. J. and MAANDERS, E. J.: 'An antenna for a satellite communication groundstation', TH-report 68-E-01, March 1968, Eindhoven University of Technology.
[5] FLUGGE, S.: 'Handbuch der Physik', Bd. 25, S.225, Springer Verlag, Berlin, 1961.
[6] THOMAS, B. MAC A: 'Theoretical performance of prime-focus paraboloids using cylindrical hybrid-mode feeds', Proc. IEE, Vol. 118, no. 11, November 1971, pp. 1539 ... 1549.
[7] CLARRICOATS, P. J. B. and SAHA, P. K.: 'Propagation and radiation behaviour of corrugated feeds', Part 1 and 2, Proc. IEE, Vol. 118, no. 9, September 1971, pp. 1167 ... 1186.
[8] ROUMEN, H. P. J. M.: 'Corrugated conical horn antennas with small flare angles', Graduate Work Report, ETA-17, 1970, Eindhoven University of Technology.
[9] JEUKEN, M. E. J. and ROUMEN, H. P. J. M.: 'Broadband corrugated conical horn antennas with small flare angles', Paper presented at International Symposium on Electromagnetic Wave Theory, (URSI) USSR, Tbilisi, September 1971.
[10] YOSHIHIRO TAKEICHI, TSUTOMU HASHIMATA and FUMIO TAKADA: 'The ring-loaded corrugated waveguide', Digest International Microwave Symposium, 1971, IEEE-GMTT.

Korte technische berichten

Het radiocontrolenet van Mexico

Ten einde zich te verzekeren van een goede organisatie van het nationale en internationale radioverkeer hebben de leden van de Internationale Telecommunicatie Unie (U.I.T.) zich gebonden aan een internationaal radioreglement. Dit reglement omvat alle technische en exploitatieve voorschriften voor het onderhouden van radiodiensten. Steunend hierop worden door de C.C.I.R.-Studiecommissies aanbevelingen geformuleerd die antwoord geven op de vragen van meer specifieke aard.

Het onderhouden van een effectieve radiocontrole ('monitoring') is één der taken, die de leden van de U.I.T. op zich hebben genomen. De belangrijkste taken van een radiocontrolecentrum zijn het vaststellen van de vulling van het radiofrequentiespectrum en het signaleren van eventueel optredende storingen. Deze taken worden uitgevoerd d.m.v. een luisterdienst, die systematisch waarnemingen verricht in het radiofrequentiespectrum.
De controle op de eigen zenders van een land is geregeld in Artikel 12 van het radioreglement en bestaat voornamelijk uit het meten van de frequentie, bandbreedte en modulatie van een zender en het meten van de door de zender veroorzaakte veldsterkte en begeleidende ongewensete stralingen. Bij het optreden van storingen in het radioverkeer moet de radiocontroledienst in staat zijn om oorzaak en plaats van de storing op te sporen en om maatregelen te nemen voor het verhelpen van de storing.

In Artikel 13 van het radioreglement hebben de landen de verplichting op zich genomen waarnemingen en metingen te verrichten voor de I.F.R.B. (International Frequency Registration Board). De technische eisen voor de radiocontrolestations worden volgens dit artikel door het C.C.I.R. opgesteld.

Van het Mexicaanse post- en verkeersministerie verkreeg Rohde & Schwarz begin 1969 de opdracht een radiocontrolenet volgens de internationale voorschriften voor geheel Mexico aan te leggen, omvattende: levering van de apparatuur, de bouw van het net en de scholing van het personeel in het bedienen der toestellen. Voor de Mexicaanse situatie betekende dit: het inrichten van vier hoofdstations, tien nevenstations en twee mobiele stations.

Het merendeel der zendinrichtingen in Mexico werkt op frequenties tussen 100 kHz en 300 MHz, waarbij het zwaartepunt ligt bij de kortegolfbanden. Men verwacht dat in de toekomst een verschuiving naar het VHF-gebied zal optreden. Op grond hiervan zijn de taken over de diverse stations als volgt verdeeld.:

- De hoofdstations zijn bedoeld voor de internationale en nationale controle, waarbij hun reikwijdte ca. 500 km is. In het HF-bereik is de reikwijdte mondiaal. De vier hoofdstations Hermosillo, San Fernando, Progreso Merida Corumel en Mexico City zijn evenals het nevenstation Tapachula met zeer gevoelige kortegolf-peilapparatuur uitgerust.
- De nevenstations zijn in de belangrijkste steden geplaatst. Zij bewaken binnen een cirkel met een straal van ca. 150 km de VHF- en UHF-uitzendingen en kunnen verder voor de MF- en HF-banden de hoofdstations ondersteunen.
- De mobiele stations voeren voornamelijk meetopdrachten uit in het VHF- en UHF-gebied. Storingsbronnen en clandestiene zenders kunnen met een mobiele eenheid ter plaatse worden opgespoord. Ook kan een dergelijke eenheid worden ingezet voor het verrichten van veldsterktemetingen en het bepalen van het verzorgingsgebied van een zender. Door middel van mobilofoons wordt contact onderhouden met de vaste stations.

De hoofdstations zijn uitgerust met vijf antennes en een antennedistributierek. Verder bevatten zij drie meetplaatsen, een panorama-ontvang- en registratieinrichting en een frequentiestandaard die wordt geijkt op de 60 kHz standaarduitzendingen van Fort Collins in de VS.

Het antennepark omvat:

- een verticale mastantenne voor het bereik 0,1 ... 30 MHz;
- een samengestelde antenne voor het bereik 1,5 ... 30 MHz; in de vorm van een verticale staaf met twee gekruiste horizontale dipolen, waarmee metingen in polarisatie-diversity kunnen worden verricht;
- een antenne voor het bereik 30 ... 120 MHz, samengesteld uit twee gekruiste verticale dipolen en een horizontale dipool;
- een dergelijke antenne voor het bereik 80 ... 330 MHz;
- een log-per antenne met bereik 30 ... 400 MHz die om een verticale as draaibaar is, gericht naar de horizon en gepolariseerd onder een hoek van 45° is opgesteld.

De meetplaatsen zijn als volgt uitgerust:

- een meetplaats voor het bereik 0,5 ... 30 MHz, voorzien van een HF-ontvanger, aangevuld met een enkelzijband demodulator, een telegrafiedemodulator, een standaard signaalgenerator, een laagfrequent spectograaf en hulpapparatuur zoals o.a. een morseschrijver, een TOR-monitor en viersporenstereobandrecorder;
- een meetplaats voor het VHF-bereik 30 ... 330 MHz, met een stuurinrichting voor de log-per antenne. Deze plaats is voorzien van een HF- en een VHF-ontvanger, een frequentie-indicator, een standaard signaalgenerator en een frequentiemeetoscillograaf. De nominale frequentie en de modulatie-index van een uitzending kunnen worden gemeten;
- een meetplaats voor het VHF/UHF-bereik 0,1 ... 900 MHz voorzien van de hiervoor benodigde ontvanger met hulpapparatuur.

In november 1970 was de te leveren apparatuur op de plaatsen van bestemming gearriveerd.

Nieuw record bij het meten van frequenties

De frequentie van een Ne-He laser is in het laboratorium van het National Bureau of Standards (USA) te Boulder zeer nauwkeurig gemeten. Men vond voor deze frequentie 88 376 245 MHz. Hiermee is een record gebroken, dat onlangs op naam van specialisten bij het M.I.T. werd gesteld.

De meettechniek, ontwikkeld door Evenson, Wells, Day en Mullen,*) komt overeen met de techniek, toegepast in de ingangstrap van de meest gangbare radio-ontvangers. Bij het experiment fungeerde een diode van bijzondere constructie als harmonischengenerator en mengtrap. De diode vermenigvuldigt de nauwkeurig bekend frequentie van een andere laser of een microgolfgenerator tot een frequentie die nabij de nog vast te stellen laserfrequentie ligt, en doet een frequentie ontstaan die het verschil is van de verkregen harmonische en de nog

*) Appl. Physics Letters 20, no. 3, 133 (Feb. 1, 1972).

te bepalen frequentie. De verschilfrequentie is enkele megahertzen hoog en kan volgens bekende methoden nauwkeurig worden gemeten.

De diode van bijzondere constructie is een microscopische verkleining van de klassieke 'catwhisker'-diode uit de beginjaren van de radio en heeft een diameter van slechts $2 \cdot 10^{-3}$ mm. De toegespitste wolfraamdraad raakt een oppervlak van nikkel, waardoor de diode ontstaat. De draad zelf is de antenne waarmee de laserstraling wordt opgevangen.

Voordat deze meting werd verricht, moesten frequenties van dergelijke hoogte door berekening worden bepaald. Men vond de frequentie door de lichtsnelheid door de golflengte te delen. De directe frequentiemeettechniek is 10^4 maal zo nauwkeurig als de golflengte-meettechniek.

De nieuw ontwikkelde techniek opent de mogelijkheid om de lichtsnelheid nauwkeuriger vast te stellen. De lichtsnelheid werd in het verleden bepaald uit een meting van golflengte en frequentie van radiogolven met een betrekkelijk lage frequentie. De nauwkeurigheid van de golflengtemeting bij die frequenties is ongeveer $3 \cdot 10^{-7}$. In het hoge infrarode gebied wordt de golflengtemeting alleen begrensd door de nauwkeurigheid waarmee de lengtestandaard bekend is. Deze nauwkeurigheid bedraagt 10^{-8}, waardoor bij dergelijke golflengten dus een 30-voudig betere nauwkeurigheid bereikt kan worden dan bij de langere golven. Langs deze weg zou de lichtsnelheid als natuurconstante dan beter kunnen worden vastgesteld.

Dit zou op zijn beurt verdere perspectieven kunnen openen voor andere wetenschappen, bijv. voor die welke de interplanetaire ruimte rondom de zon tot studie heeft en voorts voor de astronomie. Ook fysici die de lichtsnelheid in hun berekeningen als een natuurconstante nodig hebben zouden hiervan profiteren.

Milieudeskundigen zullen nieuwe vorderingen kunnen maken bij het bepalen van minutieuze hoeveelheden verontreinigingen wanneer de frequentie van precies afgestemde lasers beter kan worden vastgesteld.

Voor de telecommunicatie zou een frequentiegebied met een omvang beschikbaar kunnen komen, die 200 maal zo groot is als die van het huidige gebruikte spectrum.

Veiligheidscertificaat voor lawaai bij vliegtuigen

In de strijd tegen het vliegtuiglawaai is voor de eerste maal een meetbaan ingericht voor het bepalen van vliegtuiglawaai volgens de richtlijnen van I.C.A.O. (International Civil Aviation Organization). De meetbaan werd in Zuid-Frankrijk ingericht door Rohde & Schwarz in samenwerking met Bruel & Kjaer in de omgeving van Marseille, in opdracht van de Franse 'Service Technique de la Navigation Aerienne'. De kosten bedroegen ca. 1 miljoen gulden.

Aangenomen wordt, dat fabrikanten uit diverse landen van deze meetbaan gebruik zullen maken, wanneer zij voor de nieuwe door hen ontwikkelde vliegtuigtypen een veiligheidscertificaat tegen vliegtuiglawaai willen verkrijgen.

Het meetsysteem omvat vier meetposten, die in het verlengde van de as van de startbaan zijn opgesteld. De meetposten worden op afstand bediend en zijn uitgerust met een precisiemicrofoon, een niveau-analysator en een datamodem, Bij de landing en de start van een te meten vliegtuig wordt het niveau van het geluid dat in de meetposten wordt ontvangen geanalyseerd. Via radiokanalen worden de meetresultaten in digitale vorm doorgegeven naar een centraal opgestelde processor. De processor presenteert zijn uitkomsten in de vorm van EPNL-waarden (EPNL = Effective Perceived Noise Level). Voor documentatiedoeleinden wordt het opgevangen lawaai in de meetpost direct op een magneetband in analoge vorm vastgelegd en in de processor in digitale vorm in het geheugen opgeslagen.

Aan de meetnauwkeurigheid is grote aandacht besteed. Zo is de toegestane meetfout in het opgenomen niveau $\pm$ 1 dB, en de foutenkans voor het datakanaal 10^{-6}.

Varia

Radar-Present and Future

An international conference on 'Radar-Present and Future', organized by the Electronics Division of the Institution of Electrical Engineers, will be held in London from 23 ... 25 October 1973.

Uit het NERG

Administratie van het NERG: Postbus 39, Leidschendam. Giro 94746 t.n.v. penningmeester NERG, Leidschendam. Secretariaat van de Examencommissie-NERG: von Geusaustraat 151, Voorburg.

Ledenmutaties

Voorgestelde leden

Ir. S. M. Gresnigt, Schoolstraat 64, Vleuten.
Ir. A. Hoekstra, Willem Barentszstraat 103, Utrecht.
Ir. K. B. Klaassen, Populierenstraat 55, 's-Gravenzande.

Nieuwe leden

Ir. A. Bos, Paulus Potterstraat 6, Hoogeveen.
J. M. Schipper, Nico Bergsteynweg 109, Woudenberg.
H. L. Swaluw, Gerard Bromlaan 17, Eindhoven.

Nieuwe adressen van leden

Ir. P. K. J. van den Berg, Semmelweislaan 12, Reeuwijk.
Ir. M. W. van Batenburg, Rouboslaan 22, Voorschoten.
Prof. dr. ir. A. J. W. Duijvestijn, dr. Zamenhoflaan 212, Enschede.
Ir. H. H. Heeroma, Spechtstraat 8, Goor (O).
F. Kerkhof, Populierenstraat 8, Nederweert (L).
Ir. G. W. Lubking, Holierhoek 52, Schipluiden (ZH).
Ir. F. P. Ph. de Vries, Louis Raemaekerstraat 223, Schiedam.